A WIRELESS TRAFFIC SURVEILLANCE SYSTEM

USING VIDEO ANALYTICS

Ning Luo

Thesis Prepared for the Degree of
MASTER OF SCIENCE

UNIVERSITY OF NORTH TEXAS
May 2011

APPROVED:

Yan Huang, Major Professor
Bill Buckles, Committee Member
Robert Akl, Committee Member
Ian Parberry, Chair of the Department of
Computer Science and Engineering
Costas Tsatsoulis, Dean of College of Engineering
James Meernik, Acting Dean of the Toulouse
Graduate School

Luo, Ning. A wireless traffic surveillance system using video analytics. Master of Science (Computer Science), May 2011, 78 pp., 5 tables, 30 illustrations, bibliography, 43 titles.

Video surveillance systems have been commonly used in transportation systems to support traffic monitoring, speed estimation, and incident detection. However, there are several challenges in developing and deploying such systems, including high development and maintenance costs, bandwidth bottleneck for long range link, and lack of advanced analytics. In this thesis, I leverage current wireless, video camera, and analytics technologies, and present a wireless traffic monitoring system. I first present an overview of the system. Then I describe the site investigation and several test links with different hardware/software configurations to demonstrate the effectiveness of the system. The system development process was documented to provide guidelines for future development. Furthermore, I propose a novel speed-estimation analytics algorithm that takes into consideration roads with slope angles. I prove the correctness of the algorithm theoretically, and validate the effectiveness of the algorithm experimentally. The experimental results on both synthetic and real dataset show that the algorithm is more accurate than the baseline algorithm 80% of the time. On average the accuracy improvement of speed estimation is over 3.7% even for very small slope angles.

ACKNOWLEDGEMENTS

First I would like to express my sincere gratitude to my thesis advisor, Dr. Yan Huang. As the principle investigator of the TxDOT project which this thesis is based on, she has always been there steering the direction and providing the guidance as best as she can. Without her this thesis would not been written.

I also like to take this opportunity to thank Dr. Bill Buckles. His mentoring went far beyond this thesis and enabled me to grow intellectually during my time at the University of North Texas. I am very grateful to Dr. Robert Akl, who served on my advisory committee. I thank Yiwen, who has been my project mate and colleague for the last two years. We had a very pleasant time working together. I would like to thank my family for all the support during my study. Finally I would like to thank everyone else who has helped me and were not mentioned above.

TABLE OF CONTENTS

Page

LIST OF TABLES

LIST OF ILLUSTRATIONS

CHAPTER 1

INTRODUCTION

1.1 Motivation

We are entering an era where sensors are playing indispensable roles at almost every corner of the world. The tremendous technological advances in sensors, networking, and processing not only make the connection between the physical world and cyber-informatics world possible, but also make such connection much more affordable. It is time to investigate how these new technologies can be used in the Texas transportation systems to improve the cost-effectiveness, accuracy and timeliness of data collection.

Traffic sensors (such as video cameras and loop detectors) have been widely deployed on many freeways and arterial in major cities in Texas. They can assist in real time traffic condition visualization, travel time estimation, travel speed and volume computation, incident detection and improve the initiatives for effective traffic operation and management strategies.

Video camera sensor-based traffic surveillance is commonly used to collect video data that can help a traveler to check road congestion and assist a traffic operator visually when there is an event such as an accident. In addition, some functions have been added to video cameras to allow pedestrian information extraction [1] and vehicle classification [2], or allow a traffic operator to supervise stalled vehicles and provide timely help.

Current video traffic surveillance systems are very successful in supporting most traffic monitoring applications within Texas Department of Transportation (TxDOT). However, there are several challenging issues that have not been fully addressed by most existing systems:

(1) High development and maintenance cost

A lot of current off-the-shelf video traffic surveillance systems use CCTV (closed-circuit television) cameras connected to the communication backbone through wires such as leased phone lines (e.g. T1 lines) and Ethernet. Some can be combined with licensed radio devices purchased separately for communication. These systems are expensive in both initial investment on the hardware, installation, and long term maintenance (expensive monthly fees for leased lines).

(2) Network throughput bottleneck for long range link

Long range communication can be achieved through wireless signals. However, the throughput may suffer especially when there are a large number of cameras each transmitting real time video streams simultaneously.

(3) Lack of cost-effective and advanced analytics

Despite the rich information contained in the video, a lot of current systems still rely on on-site radar or loop detectors for some analytics tasks such as speed estimation. There are some proprietary software packages in use for video analytics such as Abacus [3], but they are expensive and only work for limited traffic conditions.

In this thesis, a new low-cost wireless video camera traffic monitoring system for TxDOT is described. The system aims at decreasing the costs of video traffic surveillance based on the following premises:

(1) Wireless communication technology is maturing and more importantly the wireless infrastructure is becoming pervasive. It is possible to link cameras via a wireless network to form a network of sensors so that the communication service does not incur long term costs to TxDOT;

(2) Video processing functions can be pushed to remote site and only video analytics information are sent to the monitoring station, which requires much less bandwidth;

(3) The analytics information are derived from video itself without resorting to additional radar or loop detectors that will incur additional implementation cost and communication overhead.

The combination of these features provides a system that promises the increased safety and system coverage while reducing costs and potentially, manpower requirements. However, configuring a low-cost system that will be able to plug into and seamlessly integrate with many of the existing information infrastructures throughout the state of Texas remains a challenging research problem. In this thesis, I thoroughly investigated and demonstrated the wireless technologies, hardware devices, software components and speed estimation algorithms that are suitable in this scenario.

1.2 Contributions

This thesis covers several fundamental aspects toward building the proposed TxDOT video traffic surveillance system, and brings together the following contributions:

- Systematic evaluation of wireless monitoring systems and technologies.

I evaluate and compare several wireless transportation surveillance systems and speed estimation algorithms. The evaluation allows us to understand the effectiveness of each technology, and provides implementation guidance for when and how to consider each technology.

- Demonstration prototype system implementation.

In this thesis, site investigation is performed and several test links are built to demonstrate the effectiveness of the system with different hardware/software configurations. I document the system development process to provide guidelines for future development.

- Novel speed-estimation analytics algorithm.

I propose a novel speed-estimation analytics algorithm that takes into consideration of roads with a slope angle. I prove the correctness of the algorithm theoretically, and validate the effectiveness of the algorithm experimentally. The experimental results on both synthetic and real dataset show that my algorithm is more accurate than the baseline algorithm 80% of the time. On average the accuracy improvement of speed estimation is over 3.7% even for very small slope angles.

1.3 Organization of This Thesis

The remainder of this thesis is organized as follows. Chapter 2 reviews related work. Chapter 3 presents the overview of system architecture, including both hardware wiring diagram and function data flow diagram, and then the details of system development, including evaluation of different wireless hardware and settings of camera. Chapter 4 proposes the novel speed estimation analytics algorithm. Finally Chapter 5 concludes the thesis and discusses future directions.

CHAPTER 2

RELATED WORK

In this chapter, I introduce the related work in two main categories: state of the art of wireless transportation surveillance systems and speed estimation (one important component of video analytics) used in transportation area.

2.1 Wireless Transportation Surveillance Systems

Traffic monitoring with cameras plays a significant role in proper road network operation, data collection and fast incident response. Compared with wired configuration, wireless communication can save a lot of infrastructural construction work, reduce the impact on the existing traffic operation system, and facilitate system maintenance. New emerging technologies not only make the wireless systems become more reliable, but also make them more affordable. As a result, many new traffic camera monitoring systems today use wireless technologies. Several representative systems are discussed in the following text.

2.1.1 Wireless Monitoring System in Irving [4]

To upgrade the traffic signal system in the city of Irving, TX, the transportation department implemented a system with 5.8GHz, 24/23 GHz and 18GHz microwaves as well as 70 CCTV cameras and message signs [4]. In order to centralize the control of 175 intersections, the engineers divided the whole area into many cells. In each cell the system applied star topology. A cluster of base stations were used at the center site, while subscribers in the field had line-of-sight wireless communication with the base stations. The city also had a wireless backbone operating at the licensed frequencies of 18-23 GHz and providing a bandwidth of 100Mbps. At a single subscriber site, the typical configuration includes a camera, a wireless device and other accessories installed inside a cabinet, as illustrated in Figure 2.1. The camera and POE (power

over Ethernet) unit of the wireless device were both powered by the power supply in the box. The camera had a build-in codec to convert analog signals into signals which can be accessed through Internet directly. The POE unit provided the wireless equipment with both power and Ethernet connection through a single Ethernet cable. The wireless device had a directional antenna facing the base station.

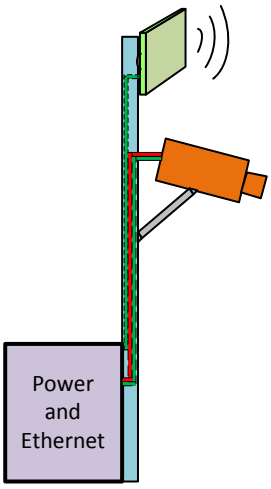

Figure 2.1 Example of Monitoring Site in Irving, TX [4]

2.1.2 Portable Detection and Surveillance System in Minnesota [5]

Portable detection and surveillance systems are often used in scenarios that require temporary yet reliable surveillance functions, such as construction sites, temporary incidents and special events. However very few off-the-shelf products are available for such purpose. One of the representative systems discussed here is developed by John Hourdakis et al. from University of Minnesota [5].

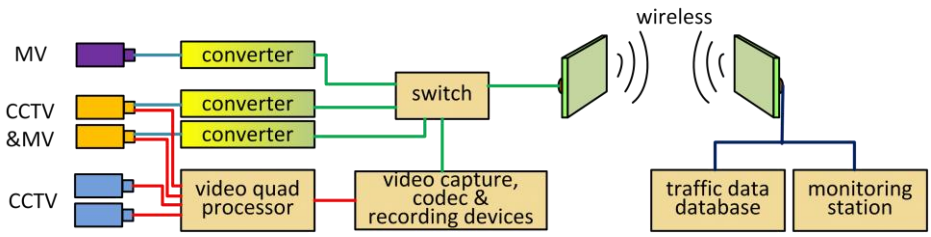

Figure 2.2 Overview of the System Developed by John Hourdakis et al. [5]

As shown in Figure 2.2, machine vision (MV) devices were deployed to detect traffic measurements. Closed-circuit televisions (CCTVs) were used to monitor real-time conditions. Since MVs used RS-485 interfaces, converters were needed to change signals from format of RS-485 to Ethernet. After conversion the signals can then be transmitted directly through general Ethernet connections. In this system, the onsite-pc has a video capture board with only one video input. Therefore a four-to-one video quad processor was used between CCTV cameras and video capture board. The processor merges the video information from four sources into one single video stream. After compression and processing, live video were fed into storage unit on site and transmitted back to the surveillance site through wireless communication channel. The monitoring side has both traffic measurement database and video streaming visualization interfaces.

To provide enough bandwidth for simultaneous data and video transmission, the system used TSUNAMI series wireless products manufactured by Proxim [6]. The frequency of the wireless link was 5.4 GHz, which was compliant with IEEE 802.16 standard, and was running frequency hopping protocol.

The above two systems still rely on traditional type of cameras with limited communication interfaces and processing capabilities. As the technology of camera evolves, more systems today are using more advanced cameras and wireless devices to form what we call “wireless camera networks” for traffic surveillance applications. The basic idea behind the wireless camera networks is to use smart cameras as sensors, which is adopted in the system described in Chapter 3.

2.1.3 Wireless Camera Network

Wireless camera networks (WCNs) are ideal candidates in today's intelligent transportation systems by leveraging wireless communication technologies, image processing algorithms, network synchronizing protocols, and data fusion mechanisms.

The WCN developed in [7] used smart cameras as sensors. The smart camera here referred to a camera combined with a powerful video processor such as a single board computer. The WCN was composed of a group of nodes and base stations. Each node collected video data from camera sensors and then sent the data to the base station. The programs running on the nodes can perform common processing tasks such as image transformation and filtering, unusual event detection etc. It was using Open Source Computer Vision Library (OpenCV) [8] to support video processing. As an example of video analytics task, authors in [7] discussed the application of the system in detecting abnormal parking and turning events. The base station received data from each node, processed the data and then transmitted the processed information to the control center. It can also send control signals to the nodes.

In the system developed by T. Semertzidis et al. [9], autonomous tracking units (ATUs) were used to obtain and process videos and images, and send the processed information to a sensor data fusion (SDF) server through wired or wireless communication channels. ATU was composed of normal CCTVs and high-performance processing units. The ATU can perform tasks such as camera calibration, background extraction, object recognition and tracking, target categorization, and coordinates transformation. The SDF server was a higher-level controller where operators can visualize the aggregated monitoring results and receive alerts for predefined events. The SDF server can perform two typical tasks: data merging and multi-object tracking. Data merging can be further classified into grid-based fusion and foreground map fusion. The

first method used grids to distinguish objects from different views of ATUs. The second method combined information from ATUs by warping and multiplying. Multi-object tracking applied multiple-hypothesis tracking (MHT) algorithm. In [9] two applications of the prototype systems were demonstrated: one scenario was airplane parking, and the other one was traffic monitoring in a tunnel on the highway.

2.1.4 Comparison of Current Systems

Among the systems discussed above, the wireless monitoring system in Irving was focused on transmission of video data without analytics information. It used star topology at the subscriber level, which is not suitable for the situation on the highway that requires a daisy chain configuration. Moreover, WiMAX technology used in this system is very expensive.

The prototype system developed in Minnesota was more portable and cost-efficient. However, the system is difficult to implement. In the field, it required converters to transmit the output of video analytic devices over TCP/IP protocol. It also used quad processor to fuse video signals from four sources, and required additional equipment to feed video into the processor on site and extra codec to compress and convert video. Moreover, the maximum transmission range of this system was only 1.7 miles.

In the wireless camera networks developed in [7], only images are stored on the server. When level of services changes, lack of original video may become a significant disadvantage. The analytics components in this system were focused on abnormal events such as wrong parking and turning. In typical traffic conditions monitoring scenario on the highway, algorithms and techniques to detect measurements such as traffic speed are also needed.

Another issue in some existing systems is the selection of cameras. For example, in [7] low-resolution laptop cameras and USB Logitech cameras were used. These cameras are not suitable

for practical applications in the transportation area. The system [9] used pre-calibrated cameras to capture videos for monitoring and processing purpose, which was less flexible than pan-tilt-zoom (PTZ) cameras in practical traffic monitoring applications.

2.2 Speed Estimation

The second category of related work is video analytics. This thesis is focused on speed estimation in particular, which is tightly coupled with camera calibration techniques. I now review several representative methods in this area.

One typical method of road speed estimation is based on individual vehicle tracking [10]-[13]. It is one of the most common speed estimation methods due to it is simplicity and robustness in free-flow traffic situation with little occlusion. Speed estimation can also be achieved without individual vehicle tracking [14]. In [14], the authors obtained one-dimensional signal in pixels for each lane in each frame, and then transformed the image signals into their counterparts in the real world. Finally they calculated the speed using cross-correlation functions. In the system described in Chapter 3, both abnormal vehicle behaviors and speed estimation need to be investigated. Therefore I follow the first type of approach to estimate speed based on vehicle tracking.

The fundamental task in speed estimation is to map the distances in the image into real world measurements. In [13], the authors selected the vehicle being tracked in several frames of images, and then calculated the transformation factor based on the actual width of the vehicle and the width in the image. For each tracked vehicle, they identified the tracking points across a collection of consecutive frames. Then they used curve fitting for these points and computed traffic measurements using derived factors or their extrapolations. The methods in [13] provided a novel way to connect the information in the image with the real world. However, the accurate

width of the vehicle in the image is not easy to measure automatically due to the influence of shadow and occlusion. Additionally, the extrapolation of factors was not proved clearly in [13].

In this thesis, I use camera calibration to associate the information in the image with the real world measurements. This is the most common method applied in the transportation research area [10]-[12]. The basic idea is to convert the coordinates in each image into coordinates in the real world through geometric transformation.

According to [15], the techniques of camera calibration can be divided into two types: methods based on one vanishing point and methods based on two vanishing points. The fundamental assumption is that the parallel lines in the real world converge in the image unless they are both perpendicular to the optical axis of the camera. The converging point is called vanishing point. Vanishing points are typically chosen to be converging point of lane marks or lines parallel to lane marks, and crossing point of lines perpendicular to the lane marks[10], [15]-[17].

Methods based on single-vanishing point usually require additional input information to perform the camera calibration. In [18], such information includes length of lane marks and lane width. In [10], the known width and length of a car on the road is used in additional to the vanishing point. The paper [16] used known width and distance from camera center projection on the ground to the nearest lane mark. In general, although this type of method requires the identification of only one vanishing point, it is less practical because additional parameters in this approach are often difficult to obtain. Moreover, this type of method introduced built-in ambiguity [15].

By contrast, methods based on two vanishing points usually only require one additional input parameter. For example, [19] and [20] proposed methods of camera calibration using two

vanishing points and lane width. In [11], the vehicle width is used instead of lane width. Similarly, if the length of an object on the road is known, camera calibration can also be accomplished using two vanishing points [15].

Almost all calibration methods discussed above assume that the road is the true horizontal plane [11], [15], [19], [20]. However, in practice it is not uncommon to see roads with slopes. Todd Nelson Schoepflin et al. discussed the influence of slopes on parameters of camera calibration and measurements [16]. They pointed out that calibration methods using two vanishing points and lane width [20] had a more than 10% relative error in distance estimation if the road slope rose up to 4 degrees. In [17], Xiao Chen He et.al. not only estimated pan angle, tilt angle, height of camera and focal length, but also computed swing angle of the camera. However, swing rotation of the camera does not have the same effect as the road slope if the image plane is not parallel to the road direction. Additionally, the input of this method was limited by the scene. It required two lane boundary marks used in the calibration to form a strict rectangle, which is difficult to be satisfied in practice. In this thesis (Chapter 4), I propose a novel calibration method that takes into the consideration of road slope with more practical assumptions.

CHAPTER 3

LOW-COST WIRELESS TRAFFIC MONITORING SYSTEM

In the previous chapter I reviewed the related work for traffic monitoring systems with wireless communication and speed estimation algorithms. In this chapter, a new wireless-camera-based traffic monitoring system for the Texas Department of Transportation (TxDOT) is proposed after leveraging the state of the art technologies. This system not only allows traditional traffic monitoring functionalities with a set of low-cost technologies, but also enables autonomous monitoring of typical situations to improve safety. I further build intelligent traffic speed estimation video analytics on top of the platform.

In this chapter, I present the system development in details. First I give an overview of the system architecture. Then I cover the evaluation of candidate technologies and implementations of a prototype system with wireless devices and a camera. In the next chapter I exemplify video analytics using a novel speed estimation algorithm.

3.1 System Overview

In this section, I show the overview of the system architecture with both hardware wiring and functional data flow diagram.

3.1.1 Hardware Wiring Diagram

As shown in Figure 3.1, each remote site traffic surveillance unit includes a network camera, a video processor and a wireless transceiver that are all connected to a local area network through a switch. The video processor can be a single border computer (SBC) or a microcomputer which can be used to perform basic camera control, on-site video processing and advanced analytics. The wireless transceiver is configured as a remote station, which relays the videos or the results of the visual analytics to the indoor monitoring station through a last-mile

wireless communication technology which in turn connects to the backbone of the Internet, a long distance wireless communication technology directly, or a multi-hop communication methods through the wireless network in daisy-chain topology.

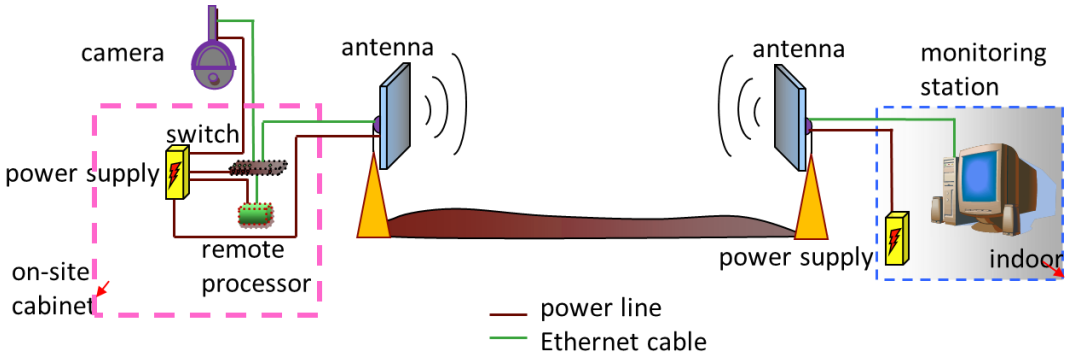

Figure 3.1 System Overview: Hardware Wiring Diagram

Each on-site unit can work independently and transmit the data to the monitoring station. All the units can also work collaboratively to serve as relaying paths and send the data over a long communication range. The monitoring station receives the visual or analytics information from each on-site remote unit through one-hop or multi-hop communications enabled by the wireless transceiver configured as a station in the same remote site. The monitoring station can store the data in a centralized place and perform actions according to the received information.

3.1.2 Function Data Flow Diagram

Let us now look at the same system architecture from a functional point of view. As Figure 3.2 shows, the functions of each system component are tightly coupled with their hardware layer capability to provide monitoring, administration, communication and analytics functionalities.

The network camera captures the real time traffic video, performs video compression (such as MPEG-4), and also provides a web-based administration interface for parameter settings and basic video viewing. The on-site video processor reads the video stream from the camera, and

processes the video information to provide analytics data services such as speed estimation statistics. Both the camera and the video processor are connected to the on-site local area network, and can be reached from the monitoring station through the wireless communication channel. The monitoring station runs several pieces of software. The monitoring station can receive videos from multiple remote sites through the live video streaming software. This software serves the same functionality as in a traditional traffic monitoring system. However, it can be turned off in favor of visualization of video analytics information whenever possible to save network bandwidth. The analytics presentation UI displays the video analytics information (such as speed and vehicle count) sent from the remote video processor. Finally the monitoring station also runs the software to monitor wireless network link quality and diagnose possible bottlenecks or failures.

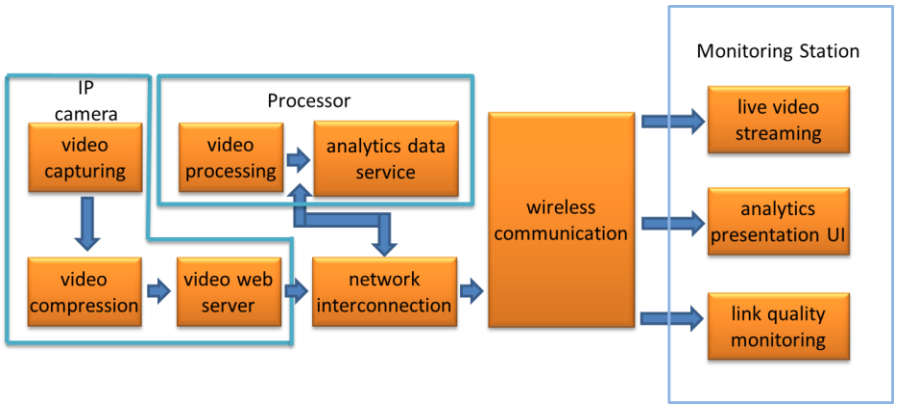

Figure 3.2 System Overview: Functional Data Flow Diagram

The above components constitute a unified system to fulfill fundamental TxDOT traffic monitoring requirements, and are implemented using low-cost technologies but will achieve autonomous video monitoring and several analytics functions.

Because this project is in progress, it has not been wholly implemented till now. In this thesis, I just present the details of components deployed. I first give an introduction of background knowledge, and then discuss the development details. I focus on candidate wireless

devices and a camera first in this chapter, and present details of analytics service provided by video processor and speed estimation in particular in the next chapter.

3.2 Background and Preliminaries

3.2.1 Architecture of Wireless Network

There are several typical wireless network topologies, such as mesh, star, tree, and line etc. For video or data transmission along a highway, the structure is typically linear. In this specific context, I can further divide configurations of wireless networks into two categories: single-hop point-to-point structure, and linear chain connection.

3.2.1.1 Single-Hop Transmission

As shown by Figure 3.3, single-hop transmission is mainly used over short-distance with no or very few obstructions (see the definition of "Fresnel zone"' below). It is typically applicable where the video or data sources are near the TMC, the backbone access point is near the camera or data processor, or there are difficulties in connecting devices in the field with wired stations.

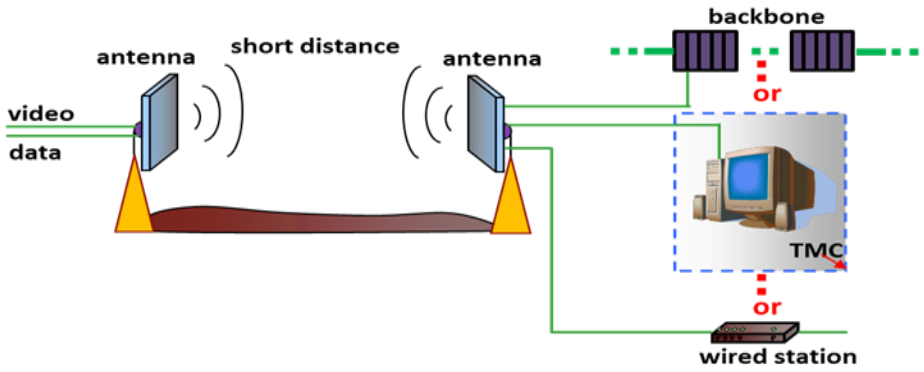

Figure 3.3 Scenario of Single-Hop Transmission

Signal attenuation affects the transmission quality and distance choice. Even if a wireless link is in line-of-sight, signal losses between transmitter and receiver may occur. Reasons include

free-space loss, cable loss, absorption, etc. Generally the majority of loss comes from the free-space loss.

- Free-space loss

Free-space loss is the loss of a wireless signal when it is transmitted in the ideal vacuum. It greatly depends on the frequency of the radio and the link distance. The following equation computes the free-space loss [21]:

$$\text{Free space loss} = 20\log_{10}\text{f} + 20\log_{10}\text{s} + 36.58 \tag{3-1}$$

In Equation 3-1, f is the frequency (in Hertz), s is the distance (in miles) between the two ends of the link. The unit of free-space loss is dB.

- Fade margin

To determine the capability of the device in handling the losses, one metric called fade margin can be used.

Fade margin is the difference between received signal strength and the minimum strength that can be captured by the receiver. This parameter indicates the reliability of a link. It can be obtained using the following formula:

$$\text{Fade margin} = \text{P}_{\text{Tx}} + \text{G}_{\text{Tx}} - \text{CL}_{\text{Tx}} - \text{S}_{\text{Rx}} + \text{G}_{\text{Rx}} - \text{CL}_{\text{Rx}} - \text{FL} \tag{3-2}$$

In Equation 3-2, P_{Tx} is the transmission power. G_{Tx} and G_{Rx} are the antenna gains of transmitter and receiver respectively. CL_{Tx} is the cable loss from the wireless transmission equipment to the transmission antenna, and CL_{Rx} is the cable loss from the wireless receiving equipment to the receiving antenna. S_{Rx} is sensitivity of a receiver whose value is usually

negative, and FL is the free-space loss. The larger the fade margin is, the more reliable the wireless link and the better the performance.

- Throughput estimation

For a single-hop wireless transmission, the formula to estimate the throughput, taking into account retransmission and timeout influences [22], is as follows:

$$\text{Throughput} = \min\left(\frac{W}{T_{RTT}}, \frac{1}{T_{RTT}\sqrt{\frac{2nR_{PER}}{3}} + T_0 \min\left(1,3\sqrt{\frac{3nR_{PER}}{8}}\right) R_{PER}(1 + 32{R_{PER}}^2)}\right) \quad (3\text{-}3)$$

In Equation 3-3, W is the maximum congestion window size;

T_{RTT} is the Round Trip Time (RTT);

n is the number of packets that are acknowledged by a single ACK;

R_{PER} is the packet error rate;

T_0 is the average timeout duration and does not include retransmission time.

3.2.1.2 Linear-Chain Transmission

A linear-chain configuration is utilized not only in long-distance transmission but also under conditions where large obstructions are on the link path.

Although line-of-sight is not a necessary factor for wireless transmission, engineers always take it into consideration. Signals under line-of-sight condition are more strong and reliable. When there are obstacles blocking the link path, one possible solution is to use a linear chain configuration. For example, in Figure 3.4 (a), antenna 4 can hardly receive video or data from antenna 1. If I add antenna 2 and 3, then (1, 2) and (3, 4) are two pairs of line-of-sight links. Data can then be transmitted between antenna 1 and 4.

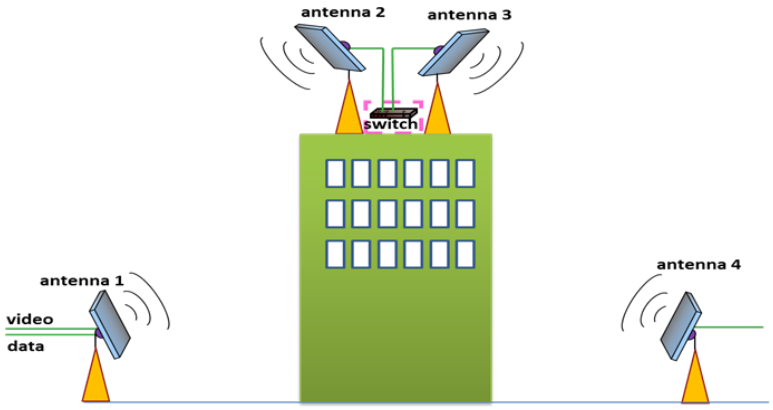

(a) Transmission with Obstructed Link Path

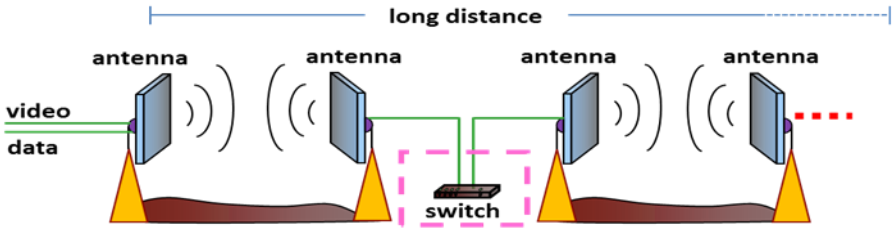

(b) Long-Distance Transmission

Figure 3.4 Scenario of Linear-Chain Transmission

Additionally, linear chain structures can be used in long-distance transmission as shown in Figure 3.4 (b). However this structure may result in significant delays if there are too many hops.

3.2.2 Antenna Pattern

An antenna pattern is a graphic description of antenna's signal spatial distribution. Based on different usages, antennas may take various forms and use different mechanisms. Examples are dipole, yagi, patch, sector antenna, etc [23]. Different antennas have different antenna patterns. For patch array antenna, an example of its pattern is depicted in Figure 3.5 [23].

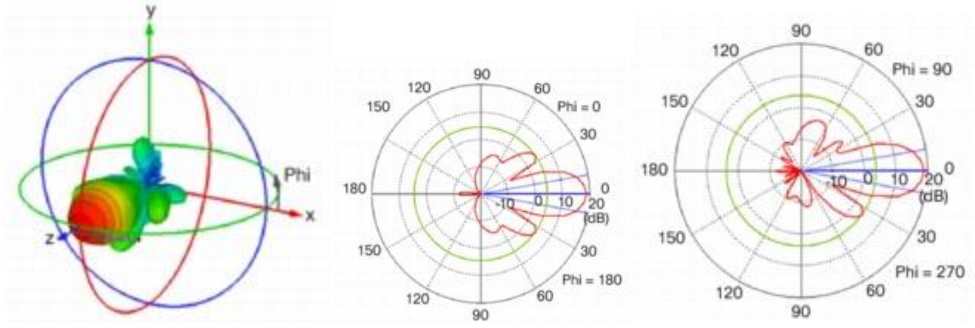

(a) 3D Pattern (b) Azimuth (c) Elevation

Figure 3.5 An Example of Antenna Pattern

As shown in Figure 3.5 (a), the radiation energy on z axis has the highest value, which tells us the best position of the peer antenna when aligned. Figure 3.5 (b) and (c) illustrate the sliced view of 3D antenna patterns through the x-z plane and y-z plane respectively. In this case, (b) is called azimuth plane and (c) is elevation plane. Both of them are in polar coordinates. If we understand the antenna pattern before setting up a wireless system, we can achieve a better antenna alignment.

3.2.3 Fresnel Zone

Fresnel zones define regions in which a particular phase difference is produced by obstructions [24]. The most important one is the first Fresnel zone occupying the most transmission power. The formula to calculate radius of this zone at any point between two termini is:

$$R = \sqrt{\frac{c}{f} * \frac{s1 * s2}{s1 + s2}} \tag{3-4}$$

In Equation 3-4, c is the velocity of wave (in meter per second), f is the frequency (in Hertz), s1 and s2 are distances (in meter) from the chosen point to each terminus. Theoretically, it is not necessary to have this zone completely obstruction free. However, when the size of the object or

part of the object in this zone is larger than 40% of radius of the zone at that point, the reduction effect is significant [25]. Figure 3.6 shows an example of Fresnel zone. Only when the size of the object or part of the object blocking this zone is larger than 40 percent of radius of the zone at that point, is the reduction effect significant [6].

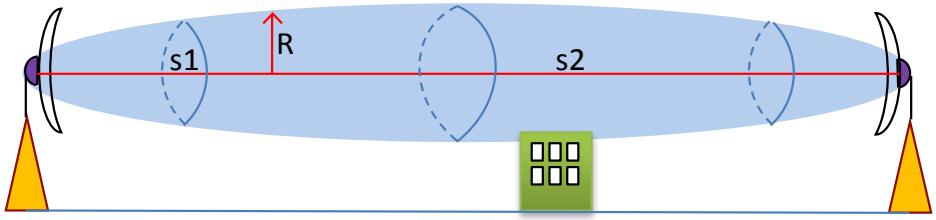

Figure 3.6 An Example of Fresnel Zone Patterns

3.2.4 Frequency Conformance and Interference

The transmission frequency is the number of cycles per second of the radio waves. It is the reciprocal of the period. Not all frequency bands are license-free. Licenses for non-free frequencies require both time and a recurring cost. However, licensed frequencies have less interference. Currently, 900MHz, 2.4GHz, and 5.8GHz are the most commonly used license-exempt frequencies. The 4.9GHz public safety frequency is reserved for Intelligent Transportation Systems (ITS) and other municipal services. Even for license-free frequencies, their usage must be subject to regulations which vary in different countries. These principles include: which wireless devices can be used in a country; which frequencies are license-free and which are not; what is the highest output power under specific conditions; in practical usage what is the relationship between antenna gain, channel width, and output power; what are the obligations of wireless network configuration, etc. In the U.S.A., the Federal Communication Commission (FCC) is responsible for regulating radio spectrum usage. For detailed information, please consult resources concerning relevant codes. One such code can be found in [26]. Fortunately, manufacturers usually have taken care of the issue to assure frequency conformance

to the regulations in each country, which makes operation of wireless devices much easier for end users. However, users have to check conformance themselves if an external antenna to be used is not integrated with a radio by the manufacturer.

License-exempt frequencies are free of charge for usage. However if there are too many devices in operation with similar frequencies in an area, there are significant interferences. Thus, checking the frequency usage at planned installation sites is essential. One may use software tools such as AirView [27] provided by Ubiquiti Networks to help in this effort. When setting up the system, avoid setting the device to operate over crowded channels.

3.3 System Development

In this section, I present the details of system development and focus on the evaluation and implementation of wireless and camera technologies.

3.3.1 Site Investigation

The first step of system development is site investigation. This is because TxDOT transportation applications require long distance transmissions, and environmental factors may influence transmission quality significantly. The input for site investigation is the geographic information of the intended locations. The main information acquired from site investigation is: distance between antenna pairs, terrain overview, possible obstructions on the link path, and minimum antenna height at each terminus.

For the configuration tests, three sites on the University of North Texas (UNT) campus are selected: two of them are inside Discovery Park (DP) campus, which is about 3 miles away from the main campus; the other one is on the roof of EESAT building on the main campus, which has two poles. The two DP sites are approximately 0.5 miles away from each other. One of them is chosen at the spot of a weather station where auxiliary devices and cables are readily available;

and the other one is on the roof of DP building. The geographic information of three selected sites is shown in Table 3.1.

Table 3.1 Geographic Information of Test Bed

Location	DP Building	EESAT (Pole 1)	EESAT (Pole 2)	DP Weather Station
Longitude	-97.15195 (-97° 9' 7.0194")	-97.15111 (-97° 9' 3.996")	-97.15109 (-97° 9' 3.9234")	-97.14997 (97° 8' 59.8914")
Latitude	33.25355 (33° 15' 12.7794")	33.21429 (33° 12' 51.4434")	33.21428 (33° 12' 51.408")	33.25690 (33° 15' 24.84")
Elevation	228.3m/749ft	226m/741.5ft	226m/741.5ft	221m / 725.1ft
Above Ground Level	15.2m/50ft	16m/52.5ft	15.5m/50.9ft	10m/32.8ft
Azimuth	358.97° (From EESAT to DP Building)		181.26°(From DP Weather Station to EESAT)	
Distance	4.365 km(2.712 miles)		4.739 km(2.945 miles)	

The testing configurations have two links. One of them is a one-hop link from EESAT (pole 1) to DP building; the other is a two-hop linear link consisting of the link from DP weather station to EESAT (pole 2), and the link from EESAT (pole 1) to DP building. The first configuration is used to compare performances of different wireless devices, and the second configuration is used for testing characteristics of linear multi-hop links.

In order to help me survey all the sites before actually deployment, I applied a variety of simulation tools. I once used Radio Mobile (downloaded from web address in [28]) to perform RF prorogation model simulation. The terrain data used in the model can be obtained from [29]. Besides, I analyzed the propagation path using a tool developed by Motorola called PTP LINKPlanner [30]. LINKPlanner is a very powerful and user-friendly network planning toolkit. It is originally designed for estimating the performance of Motorola products; however, it can also be used as a generic tool for obtaining transmission path information for any other links. It also features a Google Earth™ [31] interface to provide a bird's-eye view of the transmission

path. After entering measured geographic location data into PTP LINKPlanner, I setup the frequency and regulation parameters and obtain the profiles as shown in Figure 3.7.

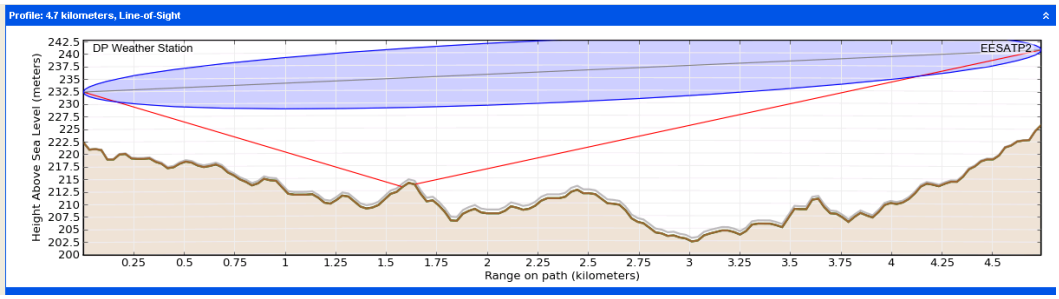

(a) DP Weather Station to EESAT

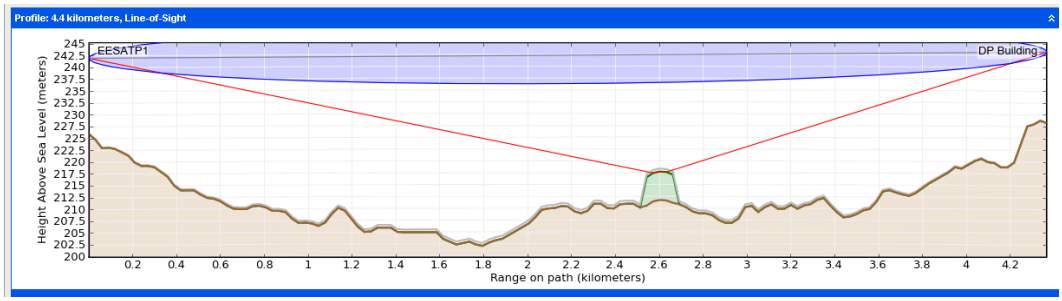

(b) EESAT to DP Building

Figure 3.7 Profiles Obtained from LINKPlanner

In Figure 3.7, the brown line outlines the contour of the terrain between two link nodes; the red lines connect antennas and the largest obstacle on the path; the blue shadowed region indicates the Fresnel zone; the green object is an obstacle above ground level. When checking the link, special attention needs to be paid on the Fresnel zone clearance, especially at high points between two paired antennas.

PTP LINKPlanner allows for mapping the link as an overlay on Google Earth™ [31]. With the help of map view, I can determine what objects may obstruct the path of communication, especially at the three points where a link is most likely to be blocked. The obstructions may have a great influence on excess path loss. However, an on-site survey of link paths is essential and cannot be totally replaced by planning tools. An on-site survey is necessary to obtain the

height of the obstructions, identify unknown blockages, and determine feasibility of the antenna height. In the test configuration, although there are buildings at three high points on the link path from EESAT to DP building, they are not in the first Fresnel zone and have little influence on signal transmission.

3.3.2 Wireless Devices

In order to choose an ideal wireless communication device for TxDOT project, I tested several representative devices and compared their performance and cost. Between the EESAT building and DP building, I developed three separate links with Motorola PTP 54300 [32], NanoStation M5 [33] and Rocket M5 [34] (with Rocket Dish [35]). I also extended the system by developing a two-hop linear system with NanoStation M5. This configuration consists of two links: one is from DP Weather Station to the EESAT building (Pole 2), and the other is from EESAT building (Pole1) to DP building.

3.3.3 PTP 54300 Configuration

3.3.3.1 Pre-Installation Configuration

Prior to installing the wireless devices, I need to have access to the device's administration interface to enter the pre-installation configuration information. For Motorola PTP 54300, the default IP address is 169.254.1.1 for master unit and 169.254.1.2 for slave unit. If the IP address of wireless equipment is unknown due to accidental change, it can be reset to the default one. The device provides a web server that can be accessed through the HTTP protocol. Using the interface, I can: validate the license key which assures the link compliance to regulations of a certain country; update the firmware if necessary; change the IP address; set the MAC address of a peer node or link name to define a link pair; identify the working mode for each device; prescribe the output power whose value should not be greater than the maximum value defined

in LINKPlanner; set the channel width which should be the same for devices at each end of the link; set link symmetry on the master unit; and enable audio tone if engineers wish to use this tone to tune the antenna, etc.

3.3.3.2 Antenna Alignment

As illustrated in the antenna pattern section, the power of the wireless signal emanating from an antenna forms a distribution pattern in the space. To achieve the best transmission result, it is essential to align the antennas carefully. Here I describe the process of antenna alignment in two stages: theoretical calculation and practical alignment.

Based on the geographical information of the sites, I can compute the azimuth and tilt angles of each antenna in the link. I used the tool provided in [36] to calculate the azimuth angle. The tilt angle can be estimated by a simple triangular transformation.

In the practical installation stage, with the help of the compass and angle scale on the antenna I can determine roughly the azimuth and tilt angle. Next I needed to perform refined adjustments. I first fixed the slave antenna and adjusted the master unit, and then fixed the master antenna and moved its counterpart. Repeat the refining steps several times until the signal strength achieves the highest value. This device also has an audio aid. When it is enabled, I can roughly judge the communication quality by the sound generated by the device. When the tone is stable with a high pitch, the link quality is acceptable. Otherwise additional adjustments are needed.

3.3.3.3 Parameter Settings

- ✓ Frequency

Motorola PTP 54300 has several options for spectrum management. In places where radar avoidance is not required, I can choose fixed frequency or intelligent dynamic frequency selection (i-DFS) options. If radar avoidance is required, I may choose dynamic frequency

selection (DFS) or DFS with i-DFS. The i-DFS mode makes devices work at the lowest level of interference. The DFS scheme changes the frequency only when radar performance is detected. The DFS with i-DFS can not only avoid radar spectrum but also select channel with the least interference automatically. For instance, at my test site there is a weather radar working at 5640MHz. I therefore chose DFS with i-DFS option to avoid radar frequency and other interference. I learned from practice that DFS with i-DFS causes improper functioning of the device for about 60-120 seconds each time the device switches frequency. Therefore it is important to setup a proper value for the threshold of frequency hopping. In this testing system I used the default value -85dBm through empirical validation.

Users can control the frequency not only by setting the spectrum management mode, but also by modifying the lower center frequency. The choices in this setting are 5478, 5480, and 5482MHz. For a 10MHz channel width, the subsequent center frequency is increased by 5MHz, starting from the user selected lower center frequency (there is an overlap between adjacent channels). Through this parameter I can change the center frequency of deployed channels. The final center frequency is chosen by the device automatically based on practical conditions. In my tests, the lower center frequency is 5480 MHz.

After setting the channel management mode and lower center frequency, the Motorola PTP 54300 device can automatically adjust the frequency to achieve the best performance.

- ✓ Transmission Symmetry

On the basis of practical requirements, I can choose 1:3, or 3:1, or 1:1 symmetry schemes if the channel width is larger than 5MHz. The main task of my wireless network is to transmit the video and/or analytics data from the field to the TMC. The link direction from video processing side to the TMC requires much more bandwidth than the reverse link direction. For testing, I

setup link symmetry to be 3:1. This allows the data rate of the link from the field to the TMC to be nearly three times of the data rate in the reverse direction. In other words, more bandwidth is used for transmitting information (video and/or analytics) from the field than that for sending commands from the TMC to the field.

- ✓ Data Rate

If dual payload mode is enabled, there are 12 coding techniques available, from 64QAM (Quadrature Amplitude Modulation) with 0.83 code rate to BPSK (Binary Phase Shift Keying) with 0.5 code rate. The device automatically selects a coding scheme and decides the data rate suitable for current circumstances. With the help of LINKPlanner, the estimated total data rate for the test configuration was 23.16Mpbs (5.68Mbps and 17.48Mbps in each direction respectively). In practice, I obtained an average speed of 19.43 Mbps (4.83 Mbps and 14.6Mbps in each direction respectively).

- ✓ Channel Width

There are three options for channel width: 5, 10, and 15MHz. As indicated in LINKPlanner, 5 MHz channel width allows very low throughput. And there is no significant throughput difference for channel width of 15MHz and 10MHz when setting other parameters as above values. Because the narrower the channel width, the less influence noise can exert on signals, I chose the channel width as 10MHz.

- ✓ Output Power

Based on the above channel width, the maximum output power suggested by LINKPlanner is 3dBm. This parameter is limited by the FCC regulations. I should set output power equal to or lower than this value. The throughput will decrease accordingly in the testing conditions if I decrease the output power. Therefore I set output power as 3dBm in the testing system.

✓ Disarming the Device

After finishing alignment and setting up the wireless link, the device should be disarmed to allow automatic modulation to take effect. The disarming of the device also disables the alignment tone, enables the programmed hopping scheme, and allows a higher data rate to come into operation. The disarming function is available through the “Disarm Installation Agent” button on the “Installation”' tab of the web administration interface. The function can also be automatically activated after the link is set up for more than 24 hours.

3.3.4 NanoStation M5 Configuration

Although Motorola PTP54300 performs well in my testing scenario, it is very expensive. One important goal of the TxDOT project is cost-effectiveness. Therefore I also tested other low-cost wireless transmission systems. Consequently, I can recommend systems with preferred tradeoffs between performance and cost. NanoStation M5 is one of the products with low cost yet great performance. In one of test configurations, I used NanoStation M5 devices and established a one-hop system and a two-hop linear system respectively.

3.3.4.1 Pre-Installation Configuration

Similar to PTP54300, NanoStation M5 also requires pre-installation configuration process. The major settings include IP address, wireless mode, SSID, frequency, channel width, and output power.

When unit is connected for the first time, the default IP address is 192.168.1.20. The default user name and password are both “ubnt”. Users can change the value of the settings after first login.

Wireless mode defines the role of a unit in a wireless network. Four modes are provided with the device: Access Point (AP), AP Wireless Distribution System (AP WDS), Station, and Station

WDS. The device functioning as a subscriber is set as “Station”, while the one bridging the wireless network and wired network is an “Access Point”. AP WDS and Station WDS are used in a wireless distribution system [37]. They are transparent on Layer 2 of an OSI network model [37]. In my test configuration, the device on the EESAT roof acts as a station and the one on the DP roof is set as an AP.

SSID is short for Service Set Identifier, which is the name of a link. Equipment on each side of a link should have the same SSID. I can also specify the AP MAC address at the station side to create a communication pair.

Using the frequency tool provided by Ubiquiti Networks [33], I can investigate the best frequency at a certain location and set this frequency at the AP side. The working frequency can be modified after a link is set up.

Channel width and output power can also be changed after a system is installed. The channel width should be the same on each side at the pre-installation stage. Output power should be sufficient to allow the two devices communicating with each other.

3.3.4.2 Antenna Alignment

The process of antenna alignment is similar to that of Motorola PTP 54300. However, NanoStation M5 does not have an audio aid tone to help in antenna alignment. The alternative is a tool in the administration interface as shown in Figure 3.8. This tool reports signal strength in real time. Thus I can align the antenna at the position until the device achieves the strongest signal strength.

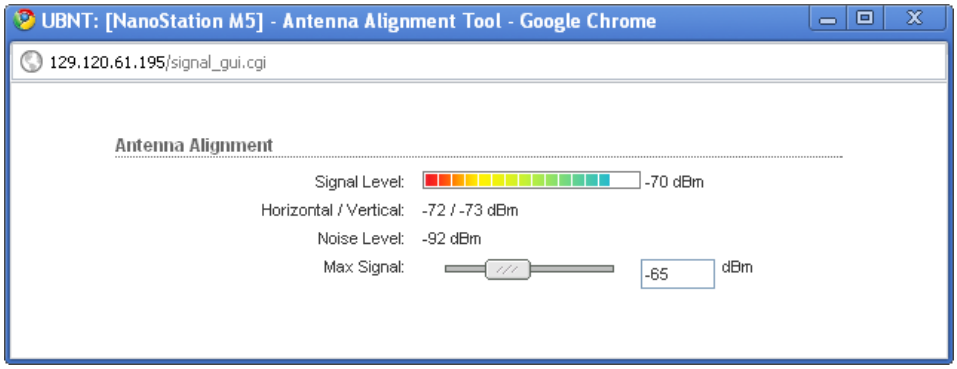

Figure 3.8 NanoStation M5 Antenna Alignment Tool

The antenna gain of NanoStation M5 is 16dbi. The vertical and horizontal polarizations are 41 and 43 degrees respectively. For practical reasons, I didn't use any kit to adjust the tilt angle of the antennas. Instead I adjusted the heights of the antennas under the line-of-sight conditions.

3.3.4.3 Parameter Settings

- ✓ Frequency

The frequency of NanoStation M5 for the test configuration is within 5470MHz-5825MHz band. I adjusted the frequency value in order to minimize the interference with other wireless systems.

Using the software AirView [38] provided by Ubiquiti Networks, I can analyze the frequency usage at each site as shown in Figure 3.9.

In Figure 3.9, the vertical axis indicates the usage of each channel measured in percentage. The usage values show the occupancy rate which takes into account quantity and energy level of wireless links in that channel. The horizontal axis is the frequency channel ranging from 5735 to 5815 MHz.

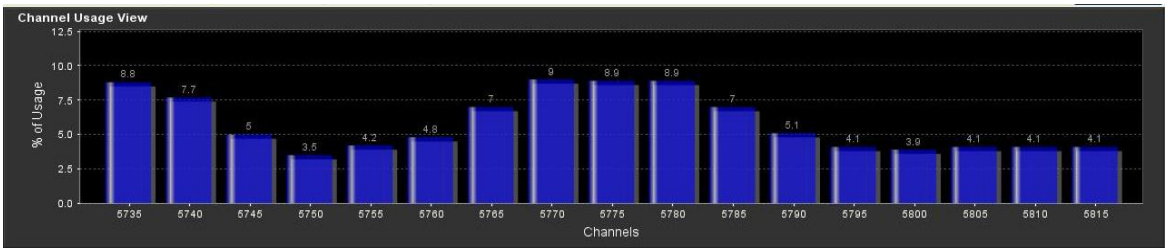

(a) From device in DP Building

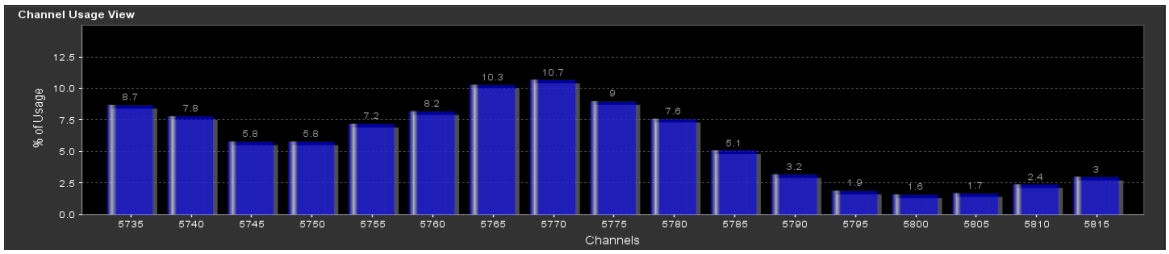

(b) From device in EESAT

Figure 3.9 Channel Usage in the NanoStation M5 Testbed

From Figure 3.9 (a), we can see that channel 154 (5770 MHz) has the highest usage, and frequencies on each side of this channel have lower usage. In Figure 3.9 (b), the usage has a similar distribution. The rule of thumb for choosing a channel is to select the one with the least interference on both sites. In the test configuration, I set the channel to be 160 (5800MHz).

✓ Data Rate

NanoStation M5 uses the 802.11a/n standard. For wireless products with standard IEEE 802.11n, the data rate is usually expressed with the Modulation and Coding Scheme (MCS) index, which represents different combinations of the number of streams, modulation method, and coding rate. For different channel widths, the same MCS index refers to different data rates. Table 3.2 shows the relationship between the MCS index and the data rate.

MCS0 and MCS8 use the Binary Phase Shift Keying (BPSK) modulation method; MCS1-2 and MCS9-10 use the Quadrature Phase Shift Keying (QPSK) modulation algorithm; MCS3-4

and MCS11-12 are based on 16 Quadrature Amplitude Modulation method (QAM) while MCS5-7 and MCS13-15 are on 64-QAM.

Table 3.2 Relationship between MCS Index and Data Rate

MCS Index	Data Rate (Mbps)			
	40MHz	20MHz	10MHz	5MHz
0	13.5	6.5	3.25	1.625
1	27	13	6.5	3.25
2	40.5	19.5	9.75	4.875
3	54	26	13	6.5
4	81	39	19.5	9.75
5	108	52	26	13
6	121.5	58.5	29.25	14.625
7	135/150	65	32.5	16.25
8	27	13	6.5	3.25
9	54	26	13	6.5
10	81	39	19.5	9.75
11	108	52	26	13
12	162	78	39	19.5
13	216	104	52	26
14	243	117	58.5	29.25
15	270/300	130	65	32.5

Fortunately, extensive experiments are not necessary to determine a sufficient data rate. The wireless equipment chooses the data rate automatically to cater to current conditions if I choose the automatic option in the administration interface.

- ✓ Channel Width

Channel width is analogous to the diameter of a pipe. The wider the channel width, the higher the throughput for the same MCS index value when the link is not saturated. However, I must consider signal strength when I choose the channel width. From Figure 3.10, we can see that the signal strength changes according to variation of channel width. Signal strength of -80 dBm or better is suggested for a reliable link. Noise floor indicates the noise level that can be used in Signal-to-Noise Ratio (SNR) calculation. The larger the gap between signal strength and noise floor, the larger the margin of the link. From practical experience, 20dBm or larger

deviation between signal strength and noise floor performs well. Therefore, I chose 10MHz as the channel width for testing.

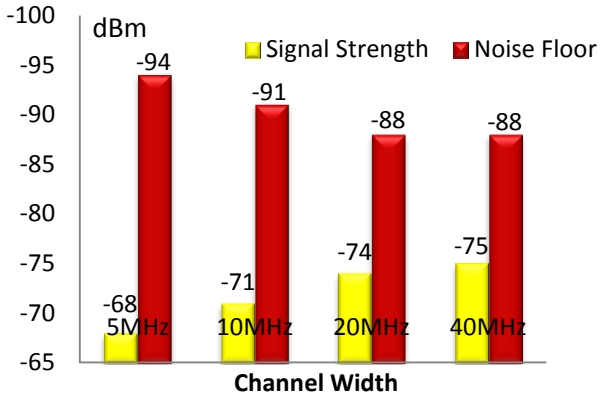

Figure 3.10 Signal Strength and Noise Floor Changes w.r.t. Channel Width

✓ Output Power

I investigated the influence of output power on signal strength, noise floor, and overall throughput. Here I set MCS index as 15 in each test and chose to change data rate automatically. Figure 3.11 gives the alterations of signal strength and noise floor with respect to output power changes. With the enhancement of output power, the noise floor remains almost the same for the same channel width, while signal strength increases.

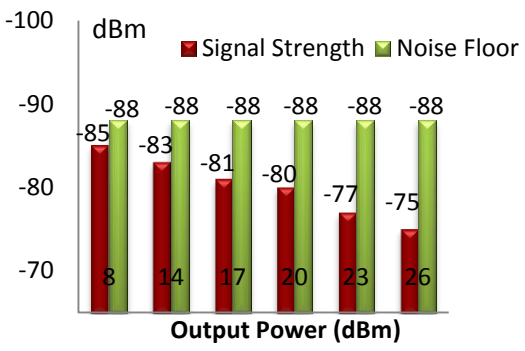

(a) 40MHz

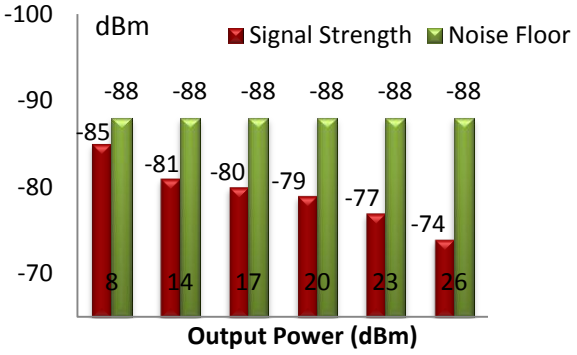

(b) 20MHz

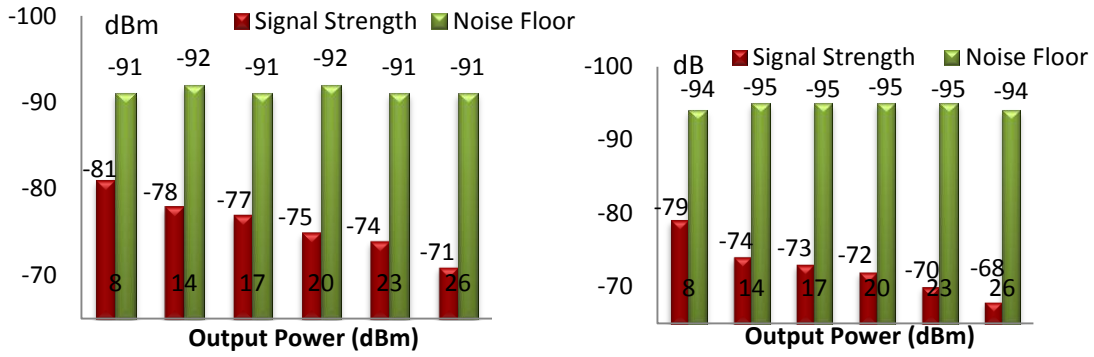

(c) 10MHz (d) 5MHz

Figure 3.11 Influence of Output Power on Signal Strength and Noise Floor

Figure 3.12 depicts the relationship between output power and throughput in the test configuration. From Figure 3.12 we can see that throughput rises with increase of output power. Consequently, output power is set as 26dBm (the maximum value) in the test system.

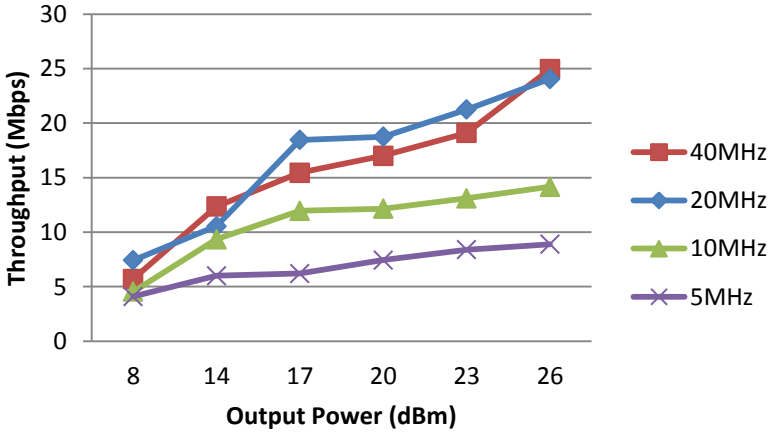

Figure 3.12 Influence of Output Power on Throughput for NanoStation M5

3.3.5 Rocket M5 Configuration

Rocket M5 is another device manufactured by Ubiquiti Networks. It can be used together with external antennas such as AirMax sectors or Rocket Dish (both of them are products of Ubiquiti Networks as well) to provide higher throughput and cover longer distances.

Additionally, Rocket M5 has a larger internal memory than NanoStation M5. Therefore it can be used in circumstances where a more powerful yet still cost-effective system is needed.

- Pre-Installation Configuration and Antenna Alignment

The pre-installation configuration for Rocket M5 is similar to that for NanoStation M5. However for antenna alignment, RocketDish 5G-30 is more difficult than NanoStation M5 because RocketDish has a higher antenna gain (30dBi) than NanoStation M5 (16dBi). The beamwidth of RocketDish 5G-30 is just 5 degrees while that of NanoStation M5 is over 40 degrees. Therefore adjusting the antenna is more challenging in this scenario. I can adjust the antenna up or down, turn left or right, and tilt upward or downward. However, rotation of antenna is not allowed.

- Parameter Settings

✓ Frequency & Channel Width

As indicated in the previous corresponding subsection, there were interferences near my testbed. But it is still competent for a larger channel width than 10 MHz. I set the frequency as 5805 and the channel width as 20 MHz.

✓ Output Power

Since this link has a relatively short distance, it is not necessary to set the output power to be the maximum value. Figure 3.13 illustrates that as the output power increases the throughput remains at almost the same level. I set the output power as 8dBm (the minimum value).

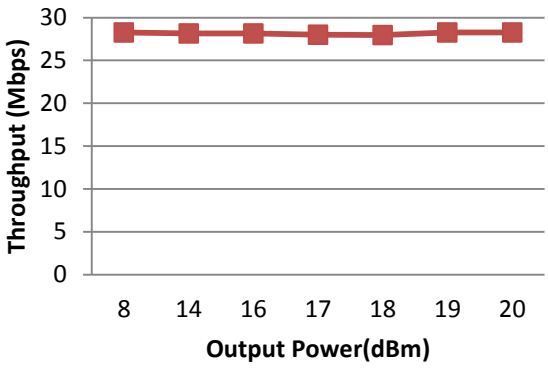

Figure 3.13 Influence of Output Power on Throughput for Rocket M5

3.3.6 Performance Comparison of Wireless Devices

So far I have discussed the configuration and testing of each wireless device. Now I compare their performance in terms of throughput.

Data rate is the nominal speed (in bits per second) in which data is transmitted across the communication pathway. Data refers to not only the user information but network information as well. The term throughput refers to the transmission speed of real user data. This parameter is the crucial measurement by which to judge a wireless system.

After I set up the three links - with Motorola PTP54300, NanoStation M5, and Rocket M5, respectively - I used Jperf [39] to test their throughputs. Jperf is written in Java and provides a graphical user interface for command-line-based throughput measurement tool Iperf [40]. Jperf/Iperf are popular tools to measure the throughput of a network using TCP or UDP protocol. The specifications of the test computer are listed in the Appendix of the thesis. In each test, I repeated the experiments and the final result is the average of two experiments.

Table 3.3 Performance Comparison of Wireless Devices

Products	Frequency (MHz)	Channel Width (MHz)	Output Power (dBm)	Throughput from EESAT to DP (Mbps)	Throughput from DP to EESAT (Mbps)
Motorola PTP 54300	5480	10	3	14.6	4.83
NanoStation M5	5800	10	26	14.5	15.1
Rocket M5+ RocketDish5G-30	5805	20	8	27.8	28.8

As can be seen from Table 3.3, Motorola PTP 54300 does not exhibit the best performance in my testing scenario. It may achieve better performance if the license was upgraded. It also provides several unique functions such as intelligent channel selection, transmission symmetry, alignment tone aid, and system monitoring, which are missing in NanoStation M5 and Rocket M5. However, NanoStation M5 and Rocket M5+ RocketDish5G-30 have competitive performances in terms of link throughput. With significantly lower cost, they are ideal candidates to build cost-effective wireless systems. I have also tested a two-hop system using the NanoStation M5. The throughput of this configuration was 10.9 Mbps.

3.3.7 Camera

The wiring of camera device is relatively simple. IP camera is chosen so that the output can be directly transmitted through the Internet without conversion equipment. I can use an Ethernet

cable to directly connect the camera with the wireless devices or through a switch. Power is supplied through a power cord.

Proper camera settings are important because they not only provide an operator acceptable quality of live video, but also conserve limited communication bandwidth.

The first important setting is the compression method. The choice must achieve satisfactory quality for the given bandwidth. Most IP camera products support motion MJPEG, MPEG-4, H.264 standard, or a combination of them. Without sacrificing quality, the size of a video file processed by H.264 may be up to 50% smaller than a file using MPEG-4, and up to 80% smaller than that produced by MJPEG [41]. However, cameras supporting H.264 are generally more expensive and less common in the current market. Cameras with MPEG-4 codec are good compromise choices. I therefore focused on this type of cameras in my system development. In the final testing, I used a camera with model number Axis 213PTZ [42] by Axis. It is a cost-efficient IP camera with MPEG-4 and motion JPEG (MJPEG) codecs support.

The Axis 213PTZ provides a web interface for parameter settings. As shown in Figure 3.14, in the main setting page, click “Video & Image” and then click “Advanced”, the “MPEG-4” settings page will be shown. I can select two types of video objects: “simple” and “advanced simple”. The simple type uses the H.263 coding method. H.263 has a lower compression rate but support viewing through QuickTime. The “Advanced Simple” option uses MPEG-4 part 2 which can function with a tool called AXIS Media Control (AMC) in Internet Explorer. AMC is an ActiveX component developed by AXIS. To conserve bandwidth, I set the type as “advanced simple”.

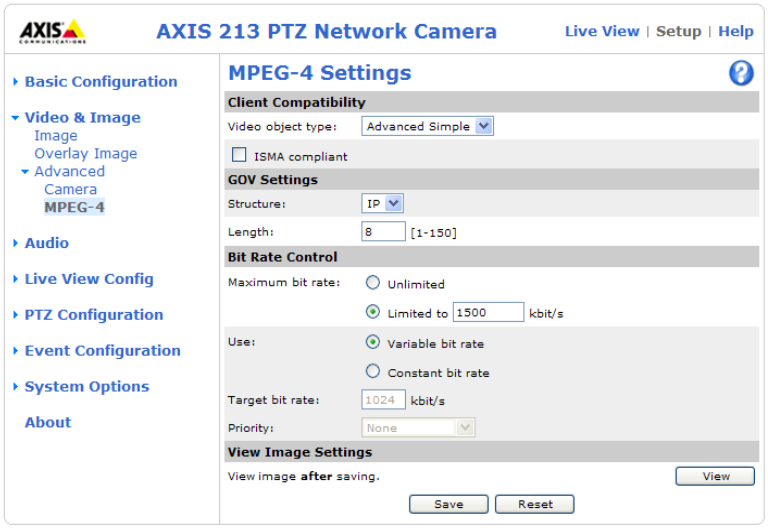

Figure 3.14 MPEG-4 Settings of Camera Axis 213 PTZ

"I frame" and "P frame" are two frame types for compressed video. "I-frame" is short for "intra-coded" frame which is independent from content in other frames when decoded. "P-frame" (short for "predicted frame") is decompressed in reference to previous frames. A video with a larger number of P-frames has a higher compression rate; however P-frame cannot be used independently. Therefore the length of Group of Video Object Plane (GOV) is set to be 8 by common practice, which means that an I-frame is always followed by seven P-frames.

Additionally, due to the limitation of wireless capacity in practical usage, I set the maximum bit rate as 1500kbps.

As shown in Figure 3.15, in "Image Settings" page, I set the resolution as 1CIF (352 x 240) and compression level as 30. In practice, 15 frames / second is acceptable for video fluency. Therefore I limited maximum frame rate to be 15 frames / second for each viewer.

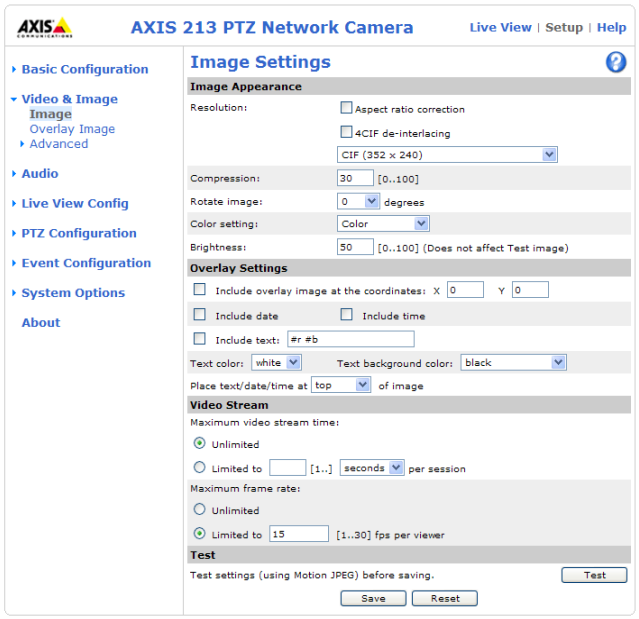

Figure 3.15 Image Settings of Camera Axis 213 PTZ

3.3.8 System Monitoring Functions

Using the wireless and camera settings introduced above, I can obtain smooth traffic videos in real time in my test cases. With the AMC component (a recommended ActiveX component used to view videos and control cameras) in Internet Explorer, the PTZ response is almost instant. I can adjust pan / tilt angles and use zoom in /out functions in the administration interface, and receive the updated video immediately.

Figure 3.16 shows several snapshots of traffic monitoring video of my test system. Due to lack of good mounting position, I had to install the camera about 90 meters (300 feet) away from the road. However I still had clear visions of cars and traffic signs.

(a)

(b)

(c)

(d)

Figure 3.16 Snapshots of Traffic Monitoring Video

To monitor the link quality of wireless communication channel, I measured system throughput and other parameters continuously over a long period.

Motorola PTP54300 provides Diagnostic Plotter for link quality monitoring as shown in Figure 3.17.

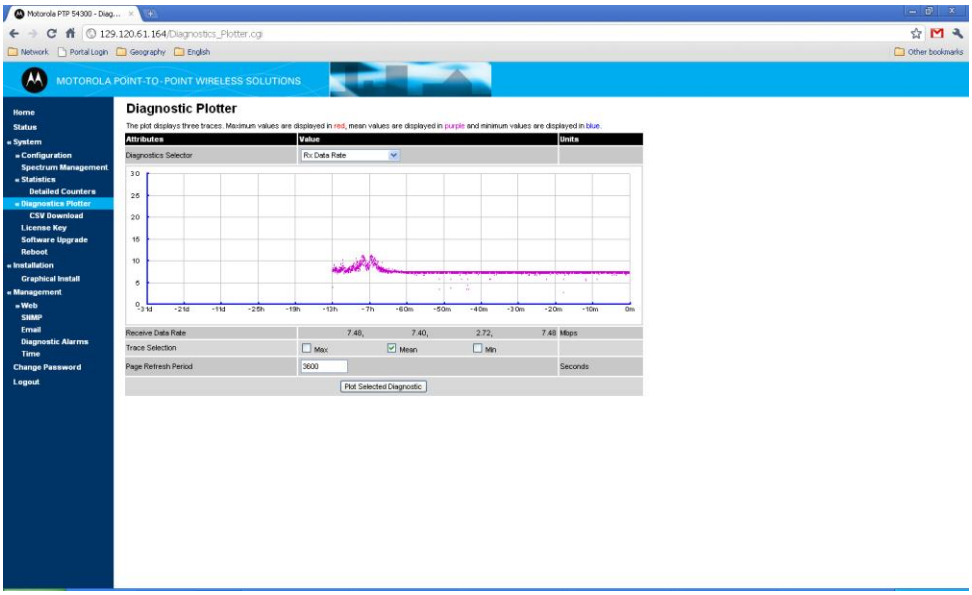

Figure 3.17 Data Rate in Diagnostic Plotter

For Ubiquiti devices, I used a tool called The Dude [43] to monitor the performance of wireless devices. The wireless equipment I used supports Simple Network Management Protocol (SNMP), which is a protocol typically used in network monitoring. Through SNMP, the Dude gets real time transmission parameters such as signal strength, transmitted packages and bytes, working data rate etc. The Dude can also visualize the data through charts over an hour, a day, a week, or even a year. Figure 3.18 and 3.19 show two screenshots of throughput and signal data measured in the Dude software.

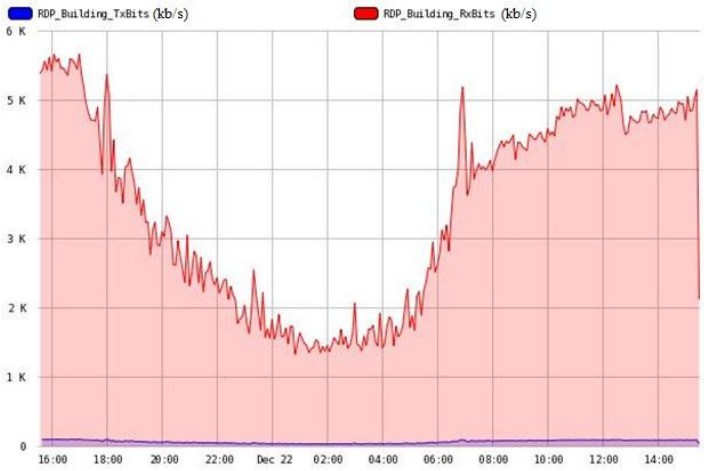

Figure 3.18 Throughput Change in a Day

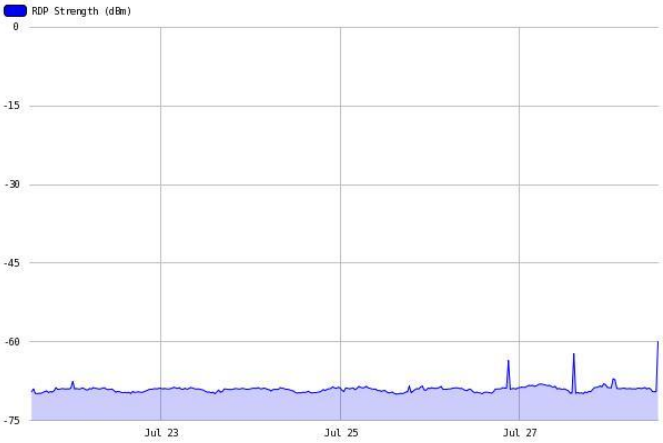

Figure 3.19 Signal Strength Change in a week

CHAPTER 4

A NOVEL SPEED ESTIMATION ALGORITHM

In Chapter 3 I have presented the details of system development, including the site investigation, the establishment of test links and choices of hardware/software configurations. In this chapter, I further discuss video analytics functions of the system. In particular I present a novel speed estimation algorithm that takes into consideration of roads with slope angles.

Speed estimation includes several steps in my system: moving object detection, camera calibration, and speed calculation. Moving object detection involves background extraction, image pre-processing, object distinguishing and moving activity recognition. One of key components of speed estimation in my system is camera calibration, which enables the transformation of distances in the real world to that in the image or vice versa. Therefore I focus on camera calibration in this chapter.

In a typical camera calibration task, I need to obtain parameters such as focal length, pan angle, tilt angle and height of camera [11], [15], [19], [20] if they are unknown. Latest IP cameras often can directly provide tilt angle parameter. Neeraj K. Kanhere et al. used the tilt angle given by the camera as the ground truth in their experiments [15]. In my camera calibration method, I also consider lane width and tilt angle as known parameters. However, unlike most of the existing methods, I have taken into consideration the road slope angles in my speed estimation algorithm.

The rest of the chapter is organized as follows: I first introduce the basic two-vanishing-point-based algorithm with known lane width; I then propose my novel speed estimation (camera calibration) algorithm that takes into consideration of roads with slopes; finally I validate my

algorithm using both indoor experiments and outdoor real traffic video and compare my method with the baseline.

4.1 Basic Method with Two Vanishing Points [15]

There are several assumptions in this method: the camera must follow the pinhole model; the road is a real level surface; and the swing angle of the camera is zero.

I first introduce the coordinate systems and notations used in this section.

In the following equations, *u* and *v* are horizontal and vertical axis of image respectively. They obey the image coordinate conventions, i.e., *u* points to the right of the image and *v* directs downward. The crossing point of *u*-and *v*-axes is at the center of the image.

The X-Y-Z coordinate system represents the 3-D real world. In this system, the origin is the projection of the camera center on the road; the Y-axis is at the intersection line of the two planes: road plane and its vertical plane containing the camera optical axis. The direction of Y-axis is toward the road. The X-axis is perpendicular to the Y-axis, and has the same direction as horizontal axis of image coordinate; the Z-axis is perpendicular to the X and Y axes and satisfies right-hand rule.

X_C'-Y_C'-Z_C' acts as an intermediate coordinate system, each axis of which has the same direction as the corresponding axes in X-Y-Z system. The origin is at the camera center.

X_C-Y_C-Z_C is the camera coordinate system whose origin is at the center of the camera. The X_C-axis and Y_C-axis are parallel to the horizontal and vertical image axis respectively. The Z_C-axis coincides with the optical axis and meets the right-hand rule.

Tilt angle is denoted by *t*. It is the angle between horizontal plane and optical axis. *p* represents the pan angle formed by the inverse Y-axis, and the traffic orientation. *f* is the camera focal length. *h* is the height of camera position in reference to X-Y plane.

Based on the notations defined above, the camera projection process from the real-world coordinates to the image coordinates takes the following three steps.

1) The transformation from X-Y-Z to X_C'-Y_C'-Z_C' coordinates is as follows:

$$\begin{aligned} X'_C &= X \\ Y'_C &= Y \\ Z'_C &= Z - h \end{aligned} \tag{4-1}$$

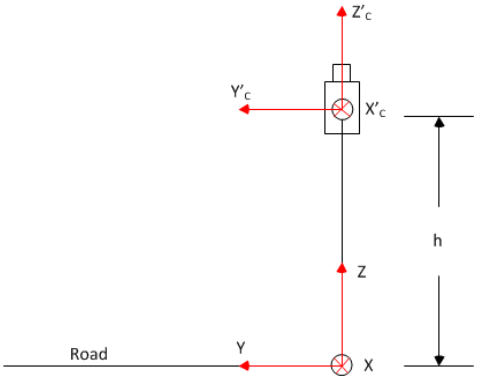

Figure 4.1 Transformation from X-Y-Z to X_C'-Y_C'-Z_C'

2) Rotate X_C'-Y_C'-Z_C' with angle *t* along X_C'-axis, then the following equations are obtained:

$$\begin{aligned} X_C &= X'_C \\ Y_C &= -Y'_C \sin(t) - Z'_C \cos(t) \\ Z_C &= Y'_C \cos(t) - Z'_C \sin(t) \end{aligned} \tag{4-2}$$

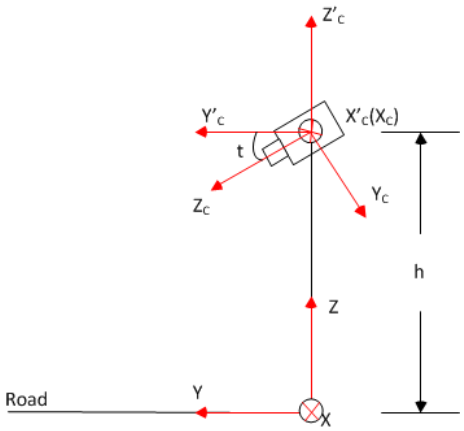

Figure 4.2 Transformation from X_C'-Y_C'-Z_C' to X_C-Y_C-Z_C

3) Based on camera pinhole model, point position on the image plane and in the camera coordinates have the below relationship:

$$u = f\frac{\mathrm{X_C}}{\mathrm{Z_C}} \tag{4-3}$$

$$v = f\frac{\mathrm{Y_C}}{\mathrm{Z_C}} \tag{4-4}$$

Substitute equation (4-1) and (4-2) into (4-3) and (4-4), and then expression (4-5) and (4-6) are derived:

$$u = f\frac{\mathrm{X}}{\mathrm{Y}\cos(t) + \mathrm{h}\sin(t)} \tag{4-5}$$

$$v = f\frac{h - \mathrm{Y}\tan(t)}{\mathrm{Y} + \mathrm{h}\tan(t)} \tag{4-6}$$

Then I solve *f*, *p*, *t* and *h*. Figure 4.3 illustrates the bird's-eye view of the road in the real world. The line L_1, L_2 and L_3 are expressed in (4-7) - (4-9) respectively in slope - intersect form,

where b_1, b_2 and b_3 are their Y-intercepts. L_1 is parallel to L_2, and perpendicular to L_3. L_1 and L_2 can be viewed as two boundary lines of a lane. L_3 can be considered as the front edge of the car or the bottom line of the windshield. An auxiliary line L_4 is also drawn. It is parallel to the X-axis and its counterpart in the image is on the line v=0. It intersects L_1 and L_2 at A and B respectively. W represents the lane width.

$$L_1: \ X = -\tan(p)\,(Y - b_1) \tag{4-7}$$

$$L_2: \ X = -\tan(p)\,(Y - b_2) \tag{4-8}$$

$$L_3: \ X = \cot(p)\,(Y - b_3) \tag{4-9}$$

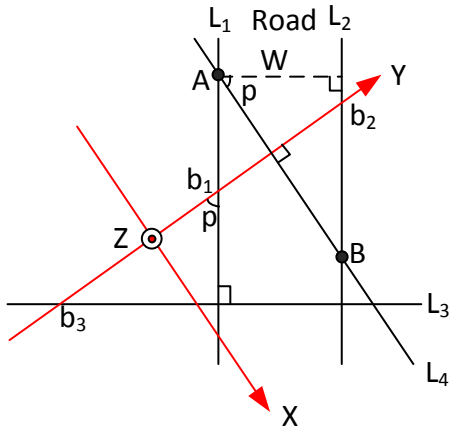

Figure 4.3 The Bird's-eye View of the Road in the Real World

Figure 4.4 shows the corresponding line relationships in the image. Line L_1', L_2', L_3'and L_4' in the image are counterparts of L_1, L_2, L_3 and L_4 respectively; the crossing points A' and B' are corresponding to A and B. After replacing X in (4-5) and (4-6) with (4-7) – (4-9) and make Y->∞, two vanishing points in the image are obtained.

$$u_0 = -f\sec(t)\tan(p)$$

$$v_0 = v_1 = -f\tan(t) \qquad (4\text{-}10)$$

$$u_1 = f\sec(t)\cot(p)$$

Solving the formulas in (4-10), focal length f, tilt angle t and pan angle p can be estimated by the following expressions:

$$f = \mathrm{sqrt}(-{v_0}^2 - u_0 u_1)$$

$$t = \arctan(-\frac{v_0}{f}) \qquad (4\text{-}11)$$

$$p = \arctan(-\frac{u_0 \cos(t)}{f})$$

Utilizing the relationship of the length of A'B', namely s, and that of AB, that is $\frac{W}{\cos(p)}$, the height of camera can also be calculated [15]:

$$h = f\frac{W\sin(t)}{s\cos(p)} \qquad (4\text{-}12)$$

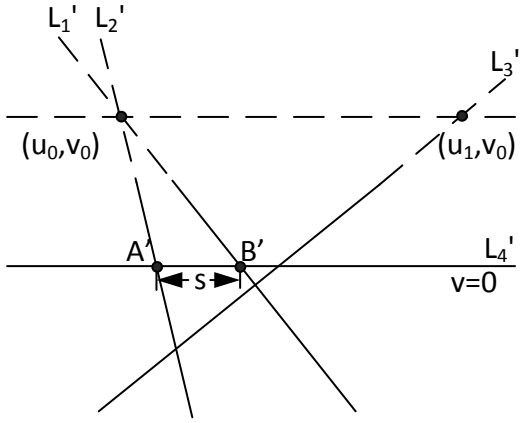

Figure 4.4 Corresponding Line Relationships in the Image

Finally the inverse perspective transformation is as follows:

$$X = h\frac{u\sec(t)}{v + f\tan(t)}$$

$$Y = h\frac{f - v\tan(t)}{v + f\tan(t)} \qquad (4\text{-}13)$$

With (4-13), I can calculate the Euclidean distance of moving objects in the real world in a specific period of time t. I divide this distance by t to get speed.

4.2 Camera Calibration for Road with Slope Angles

For the road that has a non-negligible slope, one of the assumptions in the basic algorithm no longer holds. Therefore I propose a new camera calibration method for this case.

There are seven related coordinate systems in this method: u-v, X-Y-Z, U-V-W, U'-V'-W', X'-Y'-Z', X_C'- Y_C'- Z_C', and X_C- Y_C- Z_C.

The u-v coordinate system has the same definition as described in Section 4.1.

The origin of X-Y-Z system is the intersection point of the road plane and the line which is through the camera center and vertical to the horizontal planes. The real flat plane or the horizontal plane refers the one containing the origin of this coordinate system. The Y-axis is on the intersection line of the two planes: the road plane and the vertical plane which is perpendicular to the real flat plane and contains the optical axis of camera. The direction of this axis is toward the road. The X-axis is on the road plane. It is perpendicular to the Y-axis and has positive values to the right of the Y-axis. The Z-axis is perpendicular to the X and Y axes and satisfies right-hand rule.

The angle p' is the pan angle formed by the inverse Y-axis, and the traffic orientation. The system U-V-W is rotated from X-Y-Z by $p' + \frac{\pi}{2}$ around Z-axis. Here Z-axis coincides with W-axis. The Figure 4.5 shows the relationship of X-Y-Z and U-V-W.

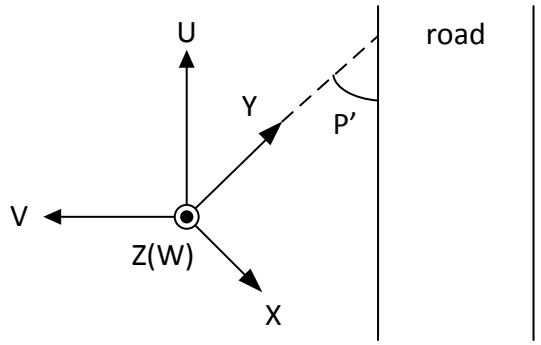

Figure 4.5 Transformation 1--The Bird's-eye View from the

Perpendicular Orientation to the Road Plane

The angle s represents the slope of the road. After turning U-V-W coordinate system by s around V-axis, the U'-V'-W' is obtained, which is demonstrated in Figure 4.6.

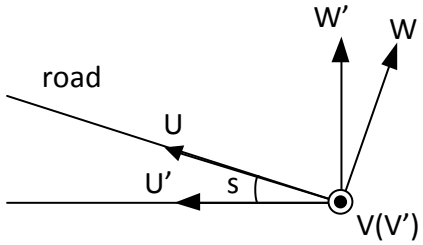

Figure 4.6 Transformation 2--The Side View of the Road

Rotating the U'-V'-W' system around W'-axis to make the new orientation of V'-axis point to the road and coincide with the intersection line of the two planes: the real flat plane and its vertical plane containing the optical axis of camera. The new coordinate system is called X'-Y'-Z'. The two sides of angle p are inverse Y'-axis and the projection of traffic direction on the real flat plane. Figure 4.7 displays this transformation.

Axes of X_C'- Y_C'- Z_C' have the same directions as those of X'-Y'-Z', but its origin is at the camera center. The side view of the camera is shown in Figure 4.8.

X_C- Y_C- Z_C has the same definition as that described in 4.1 “Basic Method with Two Vanishing Points”. Angle t, focal length f and camera height h can also be referred to in section 4.1.

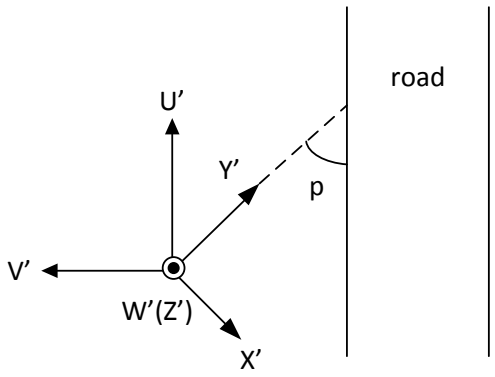

Figure 4.7 Transformation 3--The Bird’s-eye View from

the Perpendicular Direction to the Real Flat Plane

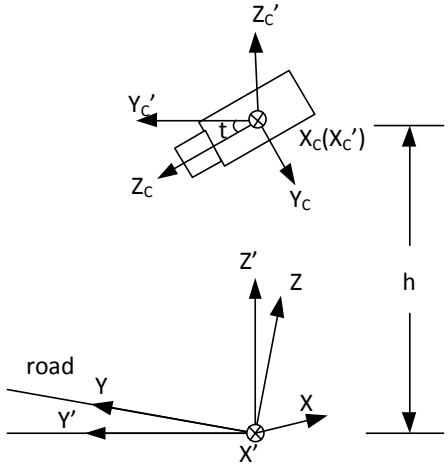

Figure 4.8 Transformation 4&5---The Side View of the Camera

The corresponding equations of transformations illustrated above are as follows:

1) Transformation from X-Y-Z to U-V-W:

$$\begin{aligned} U &= -X\sin(p') + Y\cos(p') \\ V &= -X\cos(p') - Y\sin(p') \\ W &= Z \end{aligned} \tag{4-14}$$

2) Transformation from U-V-W to U'-V'-W':

$$U' = U\cos(s) - W\sin(s)$$

$$V' = V \tag{4-15}$$

$$W' = U\sin(s) + W\cos(s)$$

3) Transformation from U'-V'-W' to X'-Y'-Z':

$$X' = -U'\sin(p) - V'\cos(p)$$

$$Y' = U'\cos(p) - V'\sin(p) \tag{4-16}$$

$$Z' = W'$$

4) Transformation from X'-Y'-Z' to X_C'- Y_C'- Z_C':

$$X_C' = X'$$

$$Y_C' = Y' \tag{4-17}$$

$$Z_C' = Z' - h$$

5) The following steps conform with (4-2)-(4-4)

6) Solve formulae (4-14)-(4-17) together with (4-2)-(4-4), make Z=0, and then the relationship from X-Y-Z to u-v is obtained:

$$u = f\frac{jX + kY}{lX + mY + h\sin(t)} \tag{4-18}$$

Where

$j = \sin(p')\cos(s)\sin(p) + \cos(p')\cos(p),$

$k = \sin(p')\cos(p) - \cos(p')\cos(s)\sin(p),$

$l = \cos(p')\sin(p)\cos(t) - \sin(p')\cos(s)\cos(p)\cos(t) + \sin(p')\sin(s)\sin(t),$

$m = \cos(p')\cos(s)\cos(p)\cos(t) + \sin(p')\sin(p)\cos(t) - \cos(p')\sin(s)\sin(t).$

$$v = f\frac{nX - qY + h\cos(t)}{lX + mY + h\sin(t)}$$

(4-19)

Where

$$n = \sin(p')\cos(s)\cos(p)\sin(t) - \cos(p')\sin(p)\sin(t) + \sin(p')\sin(s)\cos(t),$$

$$q = \cos(p')\cos(s)\cos(p)\sin(t) + \sin(p')\sin(p)\sin(t) + \cos(p')\sin(s)\cos(t).$$

To estimate the road slope s and the camera parameters, the tilt angle t and width of the road W are utilized as known values. The derivation is as follows.

Figure 4.9 illustrates the bird's-eye view of the road from the perpendicular orientation to the road plane. The line L_a and L_c are expressed in (4-20) - (4-21) respectively in slope - intersect form, where b_a and b_c are their Y-intercepts. L_a is perpendicular to L_c. L_a and L_b are two boundary lines of a lane.

$$L_a:\ X = \tan(p')(b_a - Y)$$

(4-20)

$$L_c:\ X = \cot(p')(Y - b_c)$$

(4-21)

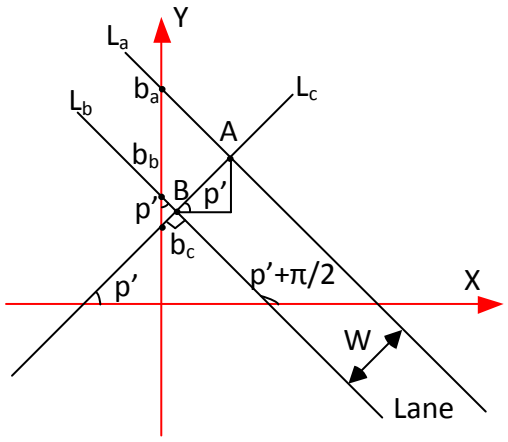

Figure 4.9 The Bird's-eye View from the Perpendicular Orientation to the Road Plane

Substitute (4-20) – (4-21) for X in (4-18) and (4-19) separately, and make $Y \to \infty$. Note that the angle p' has a relationship with the angle p: $\tan(p') = \tan(p)\cos(s)$, where s is the slope angle of road. This relationship is proven in the Appendix D. Then I obtained:

$$u_0 = -f\frac{\sin(p)}{\cos(p)\cos(t) - \tan(s)\sin(t)} \tag{4-22}$$

$$v_0 = -f\frac{\cos(p)\sin(t) + \tan(s)\cos(t)}{\cos(p)\cos(t) - \tan(s)\sin(t)} \tag{4-23}$$

$$u_1 = f\frac{1}{\tan(p)\cos(t)} \tag{4-24}$$

$$v_1 = -f\tan(t) \tag{4-25}$$

$$v_1 = Ku_1 + M \tag{4-26}$$

(u_0, v_0) are coordinates of the vanishing point of parallel lines to lane boundaries. They can be obtained by calculating the crossing point of corresponding lines of L_a and L_b in the image. (u_1, v_1) are coordinates of perpendicular lines to the lane boundaries. u_1 and v_1 satisfy (4-26), where K and M are the slope and intercept of corresponding line of L_c in the image. Solve the above equations (4-22) - (4-26), the values of u_1, v_1, f, s, p are obtained.

$$v_1 = \frac{-(v_0K + u_0) \pm \sqrt{(v_0K + u_0)^2 + 4\frac{K}{\tan^2(t)}Mu_0}}{2\frac{K}{\tan^2(t)}} \tag{4-27}$$

$$u_1 = \frac{(v_1 - M)}{K} \tag{4-28}$$

$$f = -\frac{v_1}{\tan(t)} \tag{4-29}$$

$$p = \arctan\left(\frac{fK}{\cos(t)\,(v_1 - M)}\right) \tag{4-30}$$

$$s = \arctan\left(\frac{u_0 \cos(p)\cos(t) + f\sin(p)}{u_0 \sin(t)}\right) \tag{4-31}$$

$$p' = \arctan(\tan(p)\cos(s)) \tag{4-32}$$

Because f is positive and tilt angle is normally between 0 degree and 90 degrees, v_1 is negative using formula (4-25). In the configuration of Figure 4.9, u_0, v_0 and K are usually negative. Therefore, if M has a non-negative value, the ambiguity of (4-27) can be removed by just using "+" sign before the square root symbol.

Solve (4-18) and (4-19) and make use of lane width W (see Figure 4.9), the height of camera can be computed using the following equation:

$$h = \frac{W\sin(p')}{D - E} \tag{4-33}$$

where

$$D = \frac{-eu_A \sin(t) + cu_A f\cos(t) - af\cos(t) + a\sin(t)v_A}{bcv_A - dav_A - be + deu_A + gcu_A - ga}$$

$$E = \frac{-eu_B \sin(t) + cu_B f\cos(t) - af\cos(t) + a\sin(t)v_B}{bcv_B - dav_B - be + deu_B + gcu_B - ga}$$

$$a = f(\sin(p')\cos(s)\sin(p) + \cos(p')\cos(p))$$

$$b = f(\sin(p')\cos(p) - \cos(p')\cos(s)\sin(p))$$

$$c = \cos(p')\sin(p)\cos(t) - \sin(p')\cos(s)\cos(p)\cos(t) + \sin(p')\sin(s)\sin(t)$$

$$d = \cos(p')\cos(s)\cos(p)\cos(t) + \sin(p')\sin(p)\cos(t) - \cos(p')\sin(s)\sin(t)$$

$$e = f(\sin(p')\cos(s)\cos(p)\sin(t) - \cos(p')\sin(p)\sin(t) + \sin(p')\sin(s)\cos(t))$$

$$g = f(\cos(p')\cos(s)\cos(p)\sin(t) + \sin(p')\sin(p)\sin(t) + \cos(p')\sin(s)\cos(t))$$

Then the final transformation formulae are:

$$X = \frac{1}{cu - a}(Y(b - du) - uh\sin(t)) \tag{4-34}$$

$$Y = h\frac{-eu\sin(t) + cu\, f\cos(t) - af\cos(t) + a\sin(t)v}{bcv - dav - be + deu + gcu - ga} \tag{4-35}$$

4.3 Experiments

To validate the method I proposed in the previous section, two types of experiments are implemented. I first use an indoor camera to take images for an object on a slope plane. In this experiment, I calculate the lengthwise distance, which is similar to driving distances of cars along the road. I also estimate the focal length, pan angle, height and slope of the plane where object locates, and then compare them with the real values, which are already known. The second experiment is speed estimation using real traffic video. In this experiment, I evaluated the algorithm over speeds of 52 cars and compared my method with the baseline.

4.3.1 Indoor Experiment

The focal length of the indoor camera in this series of tests is 800 pixels. The length of the object is 0.279 meter and the width is 0.215 meter.

These tests have three main configurations: in the first configuration, the pan angle is 29 degrees, the tilt angle is 45.5 degrees and the height is 2.5 meters; the second configuration has the parameters of 36 degrees, 45.5 degrees and 2.5 meters respectively; the tilt angle of the third configuration is 36 degrees, the height is 2.2 meters and the pan angle is 29 degrees. For each configuration, I vary the slope angle of the plane where the object is placed, from 2 to 4 and then to 6 degrees.

Table 4.1 gives the results of this collection of tests. In the table, the first group of columns in blue shows the ground truth information; the second group in pale mauve displays the results using the new method described in Section 4.2; the last one in yellow gives the value calculation utilizing the basic calibration method in Section 4.1. It is obvious that the length estimation has less error (in absolute value) with the new method than with the basic one. For the basic method, with the increment of the slope angle, the length estimation error increases, while slope changes do not influence much on the length calculation if using the new method.

Table 4.1 Validation Test Results

Ground Truth				Modified Method						Basic Method					
pan angle (deg)	slope angle (deg)	tilt angle (deg)	height (m)	focal length (pixel)	pan angle (deg)	slope angle (deg)	height (m)	length (m)	length deviation	focal length (pixel)	pan angle (deg)	tilt angle (deg)	height (m)	length (m)	length deviation
29	2	45.5	2.5	703	27.2	1.8	2.505	0.289	3.58%	732	26.8	46.4	2.585	0.294	5.38%
29	4	45.5	2.5	798	25.1	4.2	2.953	0.285	2.15%	867	24.3	47.8	3.155	0.296	6.09%
29	6	45.5	2.5	717	25.1	6.0	2.697	0.288	3.23%	822	23.7	48.3	3.018	0.307	10.04%
36	2	45.5	2.5	820	34.5	2.4	2.920	0.282	1.08%	863	33.8	46.9	3.068	0.289	3.58%
36	4	45.5	2.5	832	35.3	3.7	3.058	0.282	1.08%	907	34.2	47.5	3.335	0.294	5.38%
36	6	45.5	2.5	720	35.4	6.7	2.683	0.275	-1.43%	848	33.5	49.1	3.163	0.296	6.09%
29	2	36	2.2	855	25.8	2.9	2.583	0.290	3.94%	897	25.2	37.9	2.677	0.299	7.17%
29	4	36	2.2	752	25.7	5.1	2.378	0.293	5.02%	816	24.6	39.4	2.531	0.308	10.39%
29	6	36	2.2	740	25.8	7.8	2.446	0.286	2.51%	838	24.0	41.0	2.720	0.310	11.11%

4.3.2 Real Traffic Speed Estimation

In this experiment, a practical traffic video is recorded for algorithm evaluation. The tilt angle of the camera is 5.5 degrees. The lane width is 3.6 meters. I use both new method and basic method to work on the same video, and the speed estimation of each car, if recognizable by the machine, is computed. The following table lists speed estimation with different methods.

Table 4.2 Speed Estimation Results

No.	Ground Truth	New Algorithm		Basic Algorithm	
		Estimation Value	Error	Estimation Value	Error
1	55.71	51.78	-7.06%	54.15	-2.80%
2	55.71	54.06	-2.96%	56.54	1.48%
3	65.00	64.07	-1.43%	66.74	2.69%
4	65.00	66.43	2.21%	69.19	6.46%
5	65.00	67.42	3.73%	70.23	8.06%
6	66.85	67.41	0.85%	70.27	5.13%
7	65.00	64.57	-0.65%	67.21	3.40%
8	63.24	60.68	-4.05%	63.44	0.32%
9	53.18	51.18	-3.75%	53.55	0.71%
10	61.58	61.93	0.56%	64.49	4.73%
11	63.24	62.73	-0.80%	65.29	3.25%
12	58.49	57.36	-1.93%	59.74	2.14%
13	59.99	58.91	-1.80%	61.33	2.23%
14	63.24	63.93	1.09%	66.59	5.30%
15	65.00	64.49	-0.77%	67.20	3.39%
16	58.50	60.00	2.56%	62.51	6.85%
17	58.50	57.44	-1.81%	59.85	2.31%

No.	Ground Truth	New Algorithm		Basic Algorithm	
		Estimation Value	Error	Estimation Value	Error
18	55.71	55.07	-1.16%	57.37	2.98%
19	58.50	59.95	2.48%	62.46	6.76%
20	68.82	70.45	2.36%	73.36	6.60%
21	68.82	63.60	-7.59%	66.43	-3.47%
22	55.71	54.25	-2.62%	56.71	1.80%
23	54.42	55.04	1.14%	57.55	5.76%
24	55.71	54.87	-1.51%	57.38	2.99%
25	60.00	60.59	0.97%	63.35	5.58%
26	63.24	61.22	-3.20%	64.04	1.26%
27	60.00	59.85	-0.25%	62.38	3.97%
28	64.95	66.34	2.13%	69.11	6.41%
29	58.50	58.97	0.81%	61.39	4.93%
30	58.50	61.63	5.36%	64.23	9.79%
31	54.41	52.22	-4.02%	54.62	0.37%
32	58.50	59.37	1.48%	62.09	6.13%
33	55.71	55.35	-0.65%	57.82	3.79%
34	57.07	58.53	2.55%	61.20	7.23%
35	57.32	57.43	0.18%	59.78	4.28%
36	58.50	58.53	0.05%	61.01	4.29%
37	59.99	59.76	-0.39%	62.28	3.81%
38	55.71	52.76	-5.29%	55.11	-1.07%
39	61.58	62.29	1.15%	64.91	5.41%
40	55.71	59.70	7.16%	62.46	12.11%
41	58.50	58.65	0.26%	61.31	4.81%

No.	Ground Truth	New Algorithm		Basic Algorithm	
		Estimation Value	Error	Estimation Value	Error
42	57.06	56.56	-0.88%	59.17	3.69%
43	61.57	55.40	-10.02%	57.66	-6.35%
44	58.50	62.14	6.23%	64.72	10.62%
45	63.24	62.74	-0.79%	65.37	3.37%
46	60.00	61.30	2.15%	63.85	6.41%
47	50.87	50.59	-0.55%	52.69	3.58%
48	51.99	51.31	-1.31%	53.43	2.76%
49	61.57	62.43	1.40%	65.05	5.65%
50	58.50	59.90	2.40%	62.64	7.08%
51	58.49	57.47	-1.75%	60.13	2.80%
52	54.42	56.52	3.87%	59.09	8.60%

When the video is recorded, it is noticed that the road slope is small. Therefore the estimation difference between new method and basic method is not significant. The average speed of these 52 cars is 59.53 miles/second. The estimation of average speed using the new method is 59.37 miles/second, while the basic method has a result of 61.93 miles/second. For single car estimation, 80.8% of speed estimation using my method considering the slope is better than the baseline method.

CHAPTER 5

CONCLUSION AND FUTURE WORK

This thesis is focused on the development of a prototype traffic monitoring system for Texas Department of Transportation (TxDOT) with wireless communication and speed estimation. I thoroughly investigated state of art of wireless surveillance systems in transportation area, and video analytics technologies especially speed estimation algorithms, and then presented the system that features low cost wireless communication devices, improved performance over long range link as well as a novel speed estimation algorithm. The experimental results demonstrated the effectiveness of my system and the accuracy of the speed estimation algorithm.

5.1 Summary of Thesis Achievements

The research in this thesis is conducted in parallel with the development of my prototype system for TxDOT. I have made the following research and development achievements in this thesis:

- Systematic survey of state of the art wireless traffic monitoring systems and analytics technologies

In the Related Work chapter of this thesis, I evaluated and compared the relevant technologies and systems in several aspects, including wireless communication, camera sensors, and video analytics. The evaluation enabled the understanding of pros and cons of each system and provided the basis for my selection of best candidate technology to fit the need of TxDOT traffic monitoring system.

- Implementation of demonstration prototype system

Following the investigation of existing technologies, I chose the best candidate technology for the system. I performed site investigation and built several test links to demonstrate the

effectiveness of the system with the selected hardware/software configurations. I also documented the system development process to provide guidelines for future development.

- Design and implementation of a novel speed-estimation analytics algorithm

In this thesis, I also designed, implemented and validated a novel speed-estimation analytics algorithm that took into consideration of roads with slope angles. This algorithm only needs input parameters of tilt angle, lane width and two vanishing points. The experimental results on both synthetic and real dataset show that my algorithm is more accurate than the baseline algorithm 80% of the time. On average the improvement of accuracy is over 3.7% even for very small slope angles.

5.2 Future Directions

In this thesis I have presented the development of the prototype system for TxDOT traffic monitoring applications. However, toward building a full-fledged system that can be practically used in real scenario, there is still a lot of future work need to be addressed.

From the perspective of system development, I need to further enhance video processing components, including the design and development of functionalities of video processors, which is a crucial component in implementing video analytics in the system. I also need to test wireless communication channel in more scenarios, including longer communication range, more link hops and a variety of traffic conditions.

From the perspective of speed estimation, I need to further validate the algorithm with a larger real dataset and different transportation situations. Since the algorithm still requires two vanishing points, I also need to extend the algorithm for cases where two vanishing points are hard to obtain.

Appendix

A. SYSTEM DEVICES

The following devices are those used in the test systems.

Wireless Devices:

- **Nanostation M5** [8]

Manufacturer:	Ubiquiti Networks
Frequency:	5470MHz-5825MHz
Coverage:	up to 15km (9 miles)
Data Rate:	up to 150Mbps
Standard:	802.11a/n
Power/Sensitivity:	Tx Power: 802.11a: 27 dBm @ 6-24Mbps to 22 dBm @ 54Mbps, 802.11n: 27 dBm @ MCS 0 to 21dBm @ MCS 15; Sensitivity: 802.11a: -94 dBm @ 6-24Mbps to -75 dBm @ 54Mbps, 802.11n: -96 dBm @ MCS0 to -75dBm @ MCS15
Antenna:	14.6-16.1dBi
Enclosure:	Outdoor UV Stabalized Plastic
Environment:	-30° to +80°C (-22 to 176°F)

- **Rocket M5**[15] **+ RocketDish5G-30** [16]

Manufacturer:	Ubiquiti Networks
Frequency:	5470MHz-5825MHz
Coverage:	up to 50km (31miles)
Data Rate:	up to 150Mbps
Standard:	802.11a/n

Power/Sensitivity: Tx Power: 802.11a: 27 dBm @ 6-24Mbps to 22 dBm @ 54Mbps, 802.11n: 27 dBm @ MCS 0 to 21dBm @ MCS 15; Sensitivity: 802.11a: -94 dBm @ 6-24Mbps to -75 dBm @ 54Mbps, 802.11n: -96 dBm @ MCS0 to -75dBm @ MCS15

Antenna: 28.0-30.25 dBi (RocketDish**5G-30**)

Enclosure: Outdoor UV Stabalized Plastic

Environment: -30° to +75°C (-22 to 167°F)

To judge the performance of cost-effective testing wireless system, I also set up a system composed by Motorola PTP 54300 which have been used in the other TxDOT project and obtained good feedbacks.

- **PTP 54300 (Part Number: WB3151BB) [17]**

Manufacturer: Motorola

Frequency: 5470 MHz–5725 MHz

Coverage: up to 250 km (155 miles); in optional LOS up to 10km (6 miles)

Data Rate: (standard) 5 MHz: up to 13 Mbps; 10 MHz: up to 25 Mbps; 15 MHz: up to 25 Mbps

(LOS) 5 MHz: up to 18 Mbps; 10 MHz: up to 35 Mbps; 15MHz: up to 50Mbps

Power/Sensitivity: Transmission power: -18 dBm to 27 dBm;

Receiving sensitivity: -94 dBm to -69 dBm

Antenna: 23 dBi

Environment: -40° to +60°C (-40° to +140°F)

Camera

- **Axis 213 PTZ** [18]

  Name: 213 PTZ [9]+Housing 25733

  Manufacturer: Axis

  Format: 1⁄4” Interlaced CCD

  Focal Length (mm): 3.5 – 91 mm, F1.6 – F4.0

  Zoom: 26x optical/12x digital

  Angle-of-View: 1.7° – 47°

  Resolution: 160x90 to 704x576

  Minimum Illumination: Color mode: 1 lux, F1.6; IR mode: 0.1 lux, F1.6; using built-in IR light in complete darkness up to 3 m (9.8ft)

B. TESTING DEVICES

- ✓ Laptop1

  Manufacturer: Dell

  CPU: Intel Core2 Duo CPU @1.4GHz 795MHz

  RAM: 2.00GB

  Network: Broadcom 440x 10/100 Integrated Controller

- ✓ Laptop2

  Manufacturer: Dell

  CPU: Intel CPU T2050 @1.60GHz 798MHz

  RAM: 0.99GB

  Network: Broadcom 440x 10/100 Integrated Controller

C. SOFTWARE

- ✓ LINKPlanner [2]

Developer: Motorola™

Version: 2.3.10

Usage in the project: Site investigation and performance estimation for Motorola products

Link: http://motorola.wirelessbroadbandsupport.com/software/ptp/index.php

Screenshot:

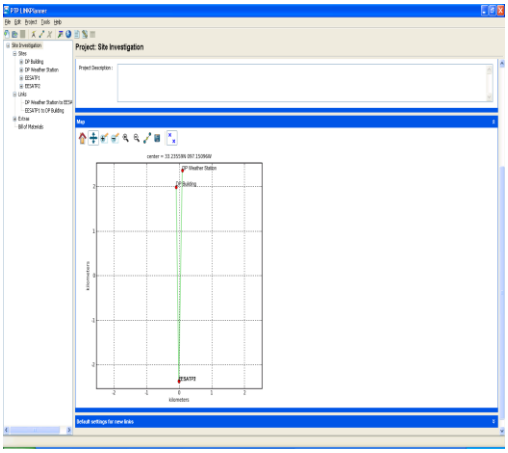

Figure C.1 Screenshot of LINKPlanner

✓ Google Earth [7]

Developer: Google™

Version: 5.2.1.1588

Usage in the project: Site investigation

Link: http://www.google.com/earth/index.html

Screenshot:

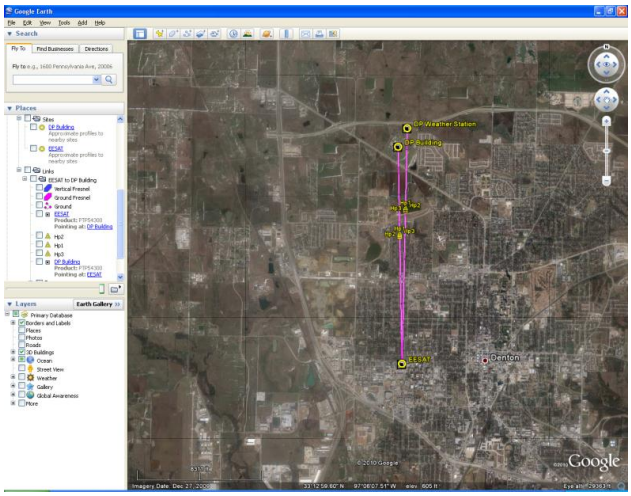

Figure C. 2 Screenshot of Google Earth

✓ Jperf [23]

Developer: Nicolas Richasse

Version: 2.02

Usage in the project: Throughput Testing

Link: http://code.google.com/p/xjperf/

Screenshot:

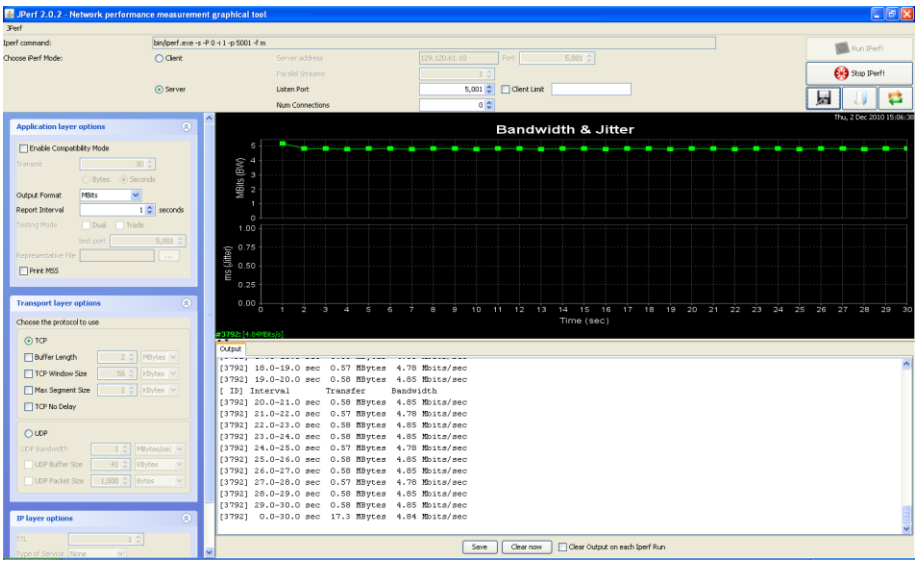

Figure C. 3 Screenshot of Jperf

✓ The Dude [12]

Developer: MikroTik™

Version: 3.6

Usage in the project: Network Monitoring

Link: http://www.mikrotik.com/thedude.php

Screenshot:

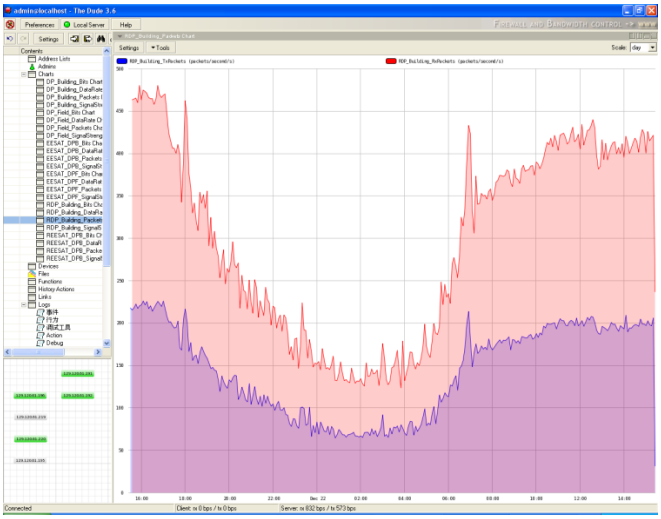

Figure C. 4 Screenshot of The Dude

D. PAN ANGLE DERIVATION FOR THE SLOPING ROAD

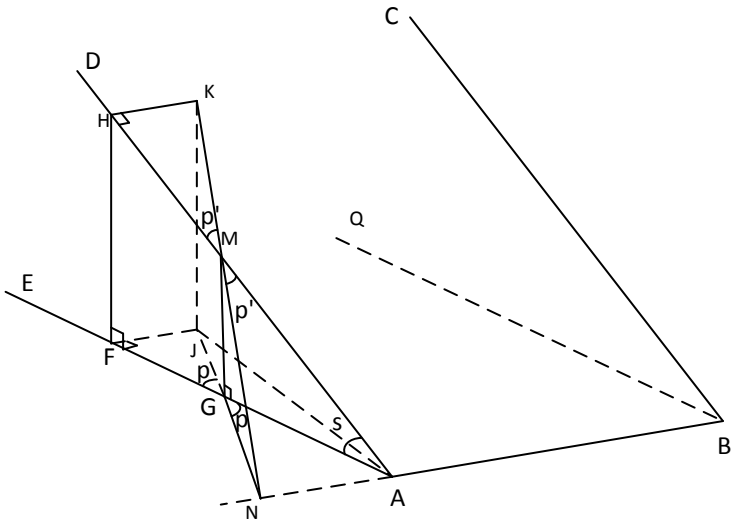

Figure D.1 Pan Angle Relationship for Sloping Roads

Suppose plane ABCD is the slanting road plane; plane ADE is vertical to the real flat plane ABQE and the plane ABCD; plane KJN is also perpendicular to the plane ABQE and contains camera optical axis, and intersects with the plane ADE at MG, with ABCD at KN, with ABQE at JN; line KJ in the plane KJN is a line perpendicular to the plane ABQE; plane FJKH is perpendicular to the plane ADE and contains the line KJ, and it has the intersection line FJ with the plane ABQE, the line HF with the plane ADE. The angle AGN is defined as p and the angle AMN is regarded as p'.

Because the plane FJKH contains the line KJ which is vertical to the plane ABQE, the plane FJKH is perpendicular to the plane ABQE too.

$\because plane\ FJKH \perp plane\ ABQE$ and $plane\ ADE \perp plane\ ABQE$

$\therefore the\ intersection\ line\ HF\ of\ FJKH\ and\ ADE \perp plane\ ABQE$

Similarly, $line\ KJ \perp plane\ ABQE$ and $line\ MG \perp plane\ ABQE$

$\because$ the lines, which are not coincide and perpendicular to a same plane, are parallel

$\therefore line\ HF \parallel line\ KJ$

Similarly, $line\ HK \parallel line\ FJ$

$\therefore quadrilateral\ FJKH\ is\ a$ parallelogram

$\therefore line\ HK = line\ FJ$

$\because line\ MG\ \perp plane\ ABQE$

$\therefore line\ MG \perp line\ AG$

Similarly, $line\ HF \perp line\ AF$, $line\ HK \perp line\ AH$ and $line\ FJ \perp line\ AF$

$$\tan(p') = \frac{HK}{MH} = \frac{HK}{AH - AM}$$

$$\tan(p) = \frac{FJ}{FG} = \frac{FJ}{AF - AG} = \frac{FJ}{AHcos(s) - AMcos(s)}$$

$\therefore \tan(p') = \cos(s)\tan(p)$

BIBLIOGRAPHY

[1] Malinovskiy, Yegor, Yao-Jan Wu and Yinhai Wang, *Video-Based Monitoring of Pedestrian Movements at Signalized Intersections*, Transportation Research Record: Journal of the Transportation Research Board, ISSN 0361-1981, Volume 2073, 2008.

[2] Guohui Zhang, Ryan Patrick Avery and Yinhai Wang, *Video-Based Vehicle Detection and Classification System for Real-Time Traffic Data Collection Using Uncalibrated Video Cameras*, Journal of the Transportation Research Board, Issue Number: 1993 ISSN: 0361-1981, 2007.

[3] Abacus™, accessed on Jan. 31, 2011, available at: http://www.iteris.com/vvd.aspx?q=10147&c=6.

[4] Sheldon Leader, *Telecommunications Handbook for Transportation Professionals -- The Basics of Telecommunications*, Technical Report of Federal Highway Administration (FHWA-HOP-04-034), 2004, available at: http://ops.fhwa.dot.gov/publications/telecomm_handbook/telecomm_handbook.pdf.

[5] John Hourdakis, Ted Morris, Panos Michalopoulos, and Kyle Wood, *Advanced Portable Wireless Measurement and Observation Station*, Report of Center for Transportation Studies in University of Minnesota(CTS 05-07), 2005, available at: http://www.cts.umn.edu/pdf/CTS-05-07.pdf.

[6] Proxim, access on January 31, 2011, available at: http://www2.proxim.com/ptpwireless-backhaul.html.

[7] Zainab Nazar Khalil Wafi, R.B. Ahmad, and R.B. Ahmad, *Wireless Cameras Network for Intelligent Traffic Surveillance System*, International Conference on Man-Machine Systems (ICoMMS), Penang, MALAYSIA, October 2009.

[8] OpenCV, access on January 31, 2011, available at: opencv.willowgarage.com/wiki.

[9] T. Semertzidis, K. Dimitropoulos, A. Koutsia, and N. Grammalidis, *Video Sensor Network for Real-time Traffic Monitoring and Surveillance*, Intelligent Transport Systems, IET, Vol. 4, Iss. 2, pp. 103–112, June 2010.

[10] Jianping Wu, Zhaobin Liu, Jinxiang Li, Caidong Gu, Maoxin Si, and Fangyong Tan, *An Algorithm for Automatic Vehicle Speed Detection Using Video Camera*, The 4th International Conference on Computer Science & Education(ICCSE '09), September 2009.

[11] Neeraj Krantiveer Kanhere, Stanley T Birchfield, and Wayne A Sarasua, *Automatic Camera Calibration Using Pattern Detection for Vision-Based Speed Sensing*, Journal of the Transportation Research Board, Issue 2086 , pp. 30-39, 2008

[12] Mei Yu, Gangyi Jiang, and Bokang Yu, *An Integrative Method for Video Based Traffic Parameter Extraction in ITS*, IEEE The Asia-Pacific Conference on Circuits and Systems (IEEE APCCAS 2000), December 2000.

[13] Daniel Jacques Benhammou, (Denver, CO, US), *United States Patent 7580547: Electronic traffic monitor*, filing date: October, 1006, available at: http://www.freepatentsonline.com/7580547.pdf.

[14] T.N. Schoepflin and D.J. Dailey, *A Correlation Technique for Estimating Traffic Speed from Cameras*, Journal of the Transportation Research Board, Issue 1855, pp. 63-73, 2003.

[15] Neeraj K. Kanhere and Stanley T. Birchfield, *A Taxonomy and Analysis of Camera Calibration Methods for Traffic Monitoring Applications*, IEEE Transactions on Intelligent Transportation Systems, Vol. 11, Iss. 2, pp. 441 - 452, June 2010.

[16] Todd Nelson Schoepflin and Daniel J. Dailey, *Algorithms for Estimating Mean Vehicle Speed Using Uncalibrated Traffic Management Cameras*, Research report of Washington State Department of Transportation (WSDOT) WA-RD 575.1, 2003.

[17] Xiao Chen He and Nelson H. C. Yung, *New Method for Overcoming Ill-conditioning in Vanishing-point-based Camera Calibration*, Journal of Optical Engineering, Vol. 46, Iss. 3, pp. 037202:1-12 , March 2007.

[18] Surendra Gupte, Osama Masoud, Robert F. K. Martin, and Nikolaos P. Papanikolopoulos, Detection and Classification of Vehicles, IEEE Transactions on Intelligent Transportation Systems, Vol. 3, No. 1, pp. 37-47, March 2002.

[19] Neeraj K. Kanhere and Stanley T. Birchfield, *Real-Time Incremental Segmentation and Tracking of Vehicles at Low Camera Angles Using Stable Features*, IEEE Transactions on Intelligent Transportation Systems, Vol. 9, Iss. 1, pp. 148 – 160, March 2008.

[20] T. N. Schoepflin and D. J. Dailey, *Dynamic camera calibration of roadside traffic management cameras for vehicle speed estimation*, IEEE on Intelligent Transportation Systems, Vol. 4, No. 2, pp. 90–98, June 2003.

[21] Free-space path loss, accessed on Oct.10, 2010, available at: http://en.wikipedia.org/wiki/Free-space_path_loss.

[22] T.K. Madsen, J. Groenbaek, J. Figueiras, H.P. Schwefel, Modelling Chain for Throughput Estimation in Wireless Networks, Vehicular Technology Conference, IEEE 69th, April 2009.

[23] Antenna Patterns and Their Meaning, accessed on Nov. 20, 2010, available at: http://www.cisco.com/en/US/prod/collateral/wireless/ps7183/ps469/prod_white_paper0900aecd806a1a3e.html.

[24] Radio Mobile - RF propagation simulation software, accessed on June 20, 2010, available at: http://radiomobile.pe1mew.nl/?Calculations:Propagation_calculation:Fresnel_zones.

[25] Roger L. Freeman, Radio System Design for Telecommunications, Wiley-Interscience, 1997.

[26] Radio Frequency Devices, accessed on Nov. 20, 2010, available at: http://ecfr.gpoaccess.gov/cgi/t/text/text-idx?c=ecfr&sid=1143b55e16daf5dce6d225ad4dc6514a&tpl=/ecfrbrowse/Title47/47cfr15_main_02.tpl.

[27] Frequency analysis tool: AirView, accessed on May 5, 2010, available at: http://ubnt.com/airview/downloads.

[28] Radio Mobile, accessed on May 11, 2010, available at: http://www.g3tvu.co.uk/Radio_Mobile_Setup.zip.

[29] Elevation data obtained by Shuttle Radar Topography Mission (SRTM), accessed on May 11, 2010, available at: http://www2.jpl.nasa.gov/srtm/.

[30] LINKPlanner, accessed on Nov. 29, 2010, available at: http://motorola.wirelessbroadbandsupport.com/software/ptp/.

[31] Google Earth, accessed on July 1, 2010, available at: http://earth.google.com/.

[32] Motorola PTP 54300/58300 Specifications, accessed on Nov. 20, 2010, available at: http://www.motorola.com/web/Business/Products/Wireless%20Networks/Wireless%20Broadband%20Networks/Point-to-Point/PTP%20300%20Series/WNS%20PTP%20300%20SS%20Updt%20072910%20r1.pdf.

[33] NanoStation M, accessed on May 5, 2010, available at: http://www.ubnt.com/nanostationm.

[34] Rocket M, accessed on Nov. 20, 2010, available at: http://ubnt.com/rocketm.

[35] RocketDish, accessed on Nov. 20, 2010, available at: http://ubnt.com/rocketdish.

[36] Distance and Azimuths Between 2 Sets of Coordinates, accessed on Nov. 20, 2010, available at: http://www.fcc.gov/mb/audio/bickel/distance.html.

[37] AirOS5.2 User Guide, accessed on Dec. 10, 2010, available at: http://ubnt.com/wiki/AirOS_5.2.

[38] Frequency analysis tool: AirView, accessed on May 5, 2010, available at: http://ubnt.com/airview/downloads.

[39] Jperf, accessed on Nov. 29, 2010, available at: http://code.google.com/p/xjperf/.

[40] Iperf software, accessed on June 2, 2010, available at: http://www.noc.ucf.edu/Tools/Iperf/.

[41] Axis technical guide to network video: Compression formats, accessed on June 4, 2010, available at: http://www.axis.com/products/video/about_networkvideo/compression_formats.htm.

[42] Data sheet of Axis 213PTZ, accessed on April 20, 2010, available at: http://www.axis.com/files/datasheet/ds_213ptz_33081_en_0909_lo.pdf.

[43] Dude software, accessed on June 3, 2010, available at: http://www.mikrotik.com/thedude.php.